NASA CONTRACTOR REPORT

NASA CR-145312

DEVELOPMENT OF AN IMPROVED METHOD OF CONSOLIDATING FATIGUE LIFE DATA

B. N. Leis and S. G. Sampath

Prepared by
BATTELLE, COLUMBUS LABORATORIES
Columbus, Ohio 43201
for Langley Research Center
under Contract No. NAS1-14171

NATIONAL AERONAUTICS AND SPACE ADMINISTRATION • WASHINGTON, D. C. • FEBRUARY 1978

1. Report No.	2. Government Accession No.	3. Recipient's Catalog No.
NASA CR 145312		

4. Title and Subtitle	5. Report Date
Development of an Improved Method of Consolidating Fatigue Life Data	February, 1978
	6. Performing Organization Code

7. Author(s)	8. Performing Organization Report No.
B. N. Leis and S. G. Sampath	G6309-1/1

9. Performing Organization Name and Address	10. Work Unit No.
Battelle Columbus Laboratories 505 King Avenue Columbus, Ohio 43201	11. Contract or Grant No. NASI-14171
	13. Type of Report and Period Covered Final Contractor Report Sept., 1975 - Aug.,1977
12. Sponsoring Agency Name and Address National Aeronautics and Space Administration Langley Research Center Hampton, Virginia 23665	14. Sponsoring Agency Code

15. Supplementary Notes

Final Report, Langley Technical Monitor: E. P. Phillips

16. Abstract The purpose of this program was to develop an improved fatigue data consolidation model that incorporates recent advances in life prediction methodology. This was a combined analytic and experimental study of fatigue of notched 2024-T3 aluminum alloy under constant-amplitude loading. Because few systematic and complete data sets for 2024-T3 were available in the literature, this program generated data for fatigue crack initiation and separation failure for both zero and nonzero mean stresses. Consolidations of these data and some from the literature are presented and discussed. The results show that the new method consolidated these data substantially better than did previous methods.

17. Key Words (Selected by Author(s))	18. Distribution Statement
cyclic deformation analysis, fatigue life prediction, stress, strain, notch, crack initiation, finite element method, data consolidation, 2024-T351 aluminum	Unclassified - Unlimited Subject Category 39 STRUCTURAL MECHANICS

19. Security Classif. (of this report)	20. Security Classif. (of this page)	21. No. of Pages	22. Price*
Unclassified	Unclassified	75	

*For sale by the National Technical Information Service, Springfield, Virginia 22151.

Page Intentionally Left Blank

CONTENTS

Page
Intentionally
Left Blank

CONTENTS (Continued)

ILLUSTRATIONS

TABLES

DEVELOPMENT OF AN IMPROVED METHOD OF CONSOLIDATING FATIGUE LIFE DATA

By B. N. Leis and S. G. Sampth
Battelle's Columbus Laboratories

SUMMARY

The purpose of this program was first to develop, evaluate and verify an improved consolidation model that incorporated recent advances in life prediction methodology and then examine the impact of this refinement on the degree of data consolidation as compared to that achieved in previous studies. Because a complete data set that included local deformation and fatigue life data for crack initiation and separation for both zero and nonzero mean stress cases was required to evaluate the fundamental assumptions and validity of the model but did not exist in the literature, a second purpose of the program was to develop these data.

Specifically, the work focused on the analysis and consolidation of data for 2024-T351 (24S-T3) aluminum smooth and notched specimens. The analysis was limited to data developed under constant amplitude cycling at stress levels less than the gross yield stress of the notched coupon. Consolidations of data available in the literature as well as that developed in this program have been presented and discussed, and the impact of the use of a refined life prediction method on the degree of consolidation examined. The results obtained show a substantially increased consolidation with this improved method.

INTRODUCTION

Fatigue design and analysis of structures involves the marriage of materials data, loads data, stress analyses and environmental considerations in accordance with some design philosophy. Usually, structural components are sized based on static strength, stability and serviceability requirements. This preliminary design is then analyzed at specific areas where fatigue may be a problem and the section properties changed accordingly, and the process repeated until the design criteria are met. Design against fatigue failure is, therefore, an iterative procedure in which a component size, shape and material are evolved such that the component serves its function for a prescribed service life at a given confidence level. In the analysis stage of the process an analytical method which predicts the fatigue life of the component is required. By contrast, in the design stage of the process an analytical method which consolidates available appropriate materials fatigue data is required. Each of these design and analysis methods embodies the same information and entails the same logic; the logic sequence, however, differs. Clearly, the more accurate the life prediction methodolgoy, the greater the consolidation of life data. It is this aspect that is examined in this report.

Recently, NASA Langley Research Center sponsored a program, the objective of which was to incorporate the then state-of-the-art life prediction methodology into a fatigue (and fatigue crack propagation) data consolidation model[1,2,3]. Although the notched specimen fatigue analysis used in this model was based on fatigue damage assessment and accumulation at the notch root, the consolidation model fell short of the degree of consolidation expected had the failure process been adequately modeled[2]. Part of the reason for this limited success may be traced to a failure to correctly compute local stresses and strains (including the effects of plasticity and biaxiality). Part of the reason may also be traced to the use of a "separation" failure criterion that included (widely varying) crack propagation periods not accounted for by the crack initiation analysis used.

More recently, life prediction methods which circumvent or directly account for the difficulties encountered in the above noted data consolidation program have evolved[4 - 8]. The purpose of this program was first to develop, evaluate

and verify an improved consolidation model that incorporated this more recent life prediction methodology and then examine the impact of this refinement on the degree of data consolidation. Because a complete data set that included local deformation and fatigue life to crack initiation and separation data for both zero and nonzero mean stress cases was required to evaluate the fundamental assumptions and validity of the model but did not exist in the literature, a second purpose of the program was to develop these data. The program, therefore, consisted of a combined analytical and experimental study, the results and discussions of which follow in the ensuing sections of this report.

Specifically, the report focuses on the analysis and consolidation of data for 2024-T351 (24S-T3) aluminum smooth and notched specimens. The analysis is limited to data developed under constant amplitude cycling at stress levels less than the gross yield stress of the notched coupon (the assumption being that strength and serviceability criteria in design preclude gross yield). The experimental details and results are first presented and discussed. Thereafter, the analytical aspects and results are presented and discussed in light of the corresponding experimental data. Consolidation of data available in the literature as well as that developed in this program is then presented and discussed and the impact of the use of a refined life prediction method on the degree of consolidation is examined. Finally, the results of this program are critically reviewed in terms of the program's objectives and the needs of the fatigue design community.

SYMBOLS

s, e	stress (MPa), strain in a smooth specimen, respectively
S, e_n	nominal stress (MPa), nominal strain in notched plates, respectively
σ, ϵ	stress (MPa), strain at a notch root, respectively
Δ	designates the peak to peak value of the corresponding quantity
K_f	fatigue notch factor

K_t	theoretical stress concentration factor
K_f^t	theoretical fatigue notch factor
P	Neuber parameter
T, Py	far field tractions and local yield load for notched plate (sheet) specimen, N
R	algebraic ratio of minimum to maximum stress
E, E_t, E*	elastic modulus, tangent modulus and effective modulus defined by $3E/2\ (1 + \nu)$ where ν is Poissons ratio, MPa
$\underset{\sim}{X}$	designates the tensorial nature of the corresponding quantity, X say
$\bar{X}$	designates the equivalent value of X say, based on the second invariant of the corresponding tensor
D_R	damage per reversal
N, 2N, R_f	cycles and reversals of loading
ℓ	crack length, mm
x, y, z	cartesian coordinates
θ, r, z	cylindrical coordinates
$\theta\theta$, rr, zz	as subscripts designate components in the θ, r and z directions on the θ, r and z faces
1, 2, 3	as subscripts designate principal components; $1 > 2 > 3$
t, e, p	as superscripts designate total elastic and plastic components
mx, mn	as subscripts designate maximum and minimum values
i, p, f	as subscripts designate initiation, propagation and fracture values

EXPERIMENTAL ASPECTS

BACKGROUND

The fatigue literature abounds with experimental data over a broad range of temperatures, specimen geometries and stress concentration factors, stress levels (lives to failure), control conditions, and materials. Yet no single data set needed to verify the assumptions and validate the life prediction method simultaneously satisfied the following criteria: (1) measured both crack initiation (crack length, ℓ_i, less than 0.1 mm, say) and life to separation, (2) measured notch root strain, (3) tested a notched specimen configuration with a locally plane stress state, (4) developed both fully reversed and nonzero mean stress data, (5) studied the behavior over a life range that encompassed both local elastic and local inelastic deformation response, and (6) developed data in both smooth and notched samples. (A few authors have simultaneously met as many as five of these criteria, most notably Crews[4] and Leis, et al[5-8].) Consequently, an experimental program designed to simultaneously meet these criteria was performed as a part of this program.

The present program simultaneously met these criteria by measuring the maximum principal strain at the notch root using a specially designed notch root extensometer in a thin notched plate in conjunction with an eddy current device located in the notch to detect initiation. (This instrumentation is detailed later in this section.) These measurements were made over a broad range of lives under test conditions that encompassed both smooth and notched samples tested under both fully reversed and nonzero mean stress constant amplitude histories, as detailed in Table 1.

MATERIALS AND SPECIMENS

The material used in this investigation was wrought aluminum alloy sheet, supplied by the Langley Research Center in blanks nominally 30.5 cm by 88.9 cm, 2.3 mm thick. A total of ten blanks numbered A121S1 to A130S1 were shipped. According to Langley Research Center (NACA) records[9], the material provided was obtained from blanks designated as spares taken from sheets numbered 121 to 130. These sheets are a part of the 135 sheets obtained by

TABLE 1. - EXPERIMENTAL PROGRAM

Specimen Type	Test Type	Control Condition	Specimens Committed	Instrumentation			
				Nominal		Local	
				Strain/ Stroke	Stress	Strain	Initiation
Smooth	Monotonic Tension	Strain/Stroke	3	✓	✓	--	--
Smooth	Fully Reversed	Strain	12	✓	✓	--	--
Smooth	Tensile Mean Stress	Strain	7	✓	✓	--	--
Notched	Monotonic Tension	Stroke	1	✓	✓	✓	--
Notched	Fully Reversed	Load	15	✓	✓	✓	✓
Notched	Tensile Mean Stress	Load	14 (10)	✓	✓	✓	✓
			14 (4)	✓	✓	--	--

Langley Research Center since the early 1950's. The blanks were painted on both sides with a zinc chromate primer and bore the designation 24S-T. This designation was the forerunner of 2024-T3 (or T351, depending on the mill prestretch history)[10]. NACA records indicate the long direction of the blanks is aligned with the grain (rolling direction) of the material. Extensive fatigue resistance data for this material have been developed for smooth specimens along with monotonic tension data, as summarized in Reference 11. Equally extensive notched specimen fatigue resistance data have been developed, as reported in Reference 12. Other sparse but relevant fatigue life and cyclic deformation data for this material have been developed as reported in References 1 and 4.

As indicated in the test matrix, Table 1, the experimental program made use of both smooth and notched sheet specimens tested under strain and load control, respectively. All smooth specimens were sheared nominally 14.61 cm long by 4.64 cm wide. They tapered symmetrically in planform through a 2.54 cm radius into a uniform test section (gage length) 1.91 cm long by nominally 1.78 cm wide. The last 0.381 mm of the width of the test section was removed by successive cuts of about 0.0254 mm in an effort to avoid inducing surface residual stresses. Of the 23 smooth specimens utilized in the program, numbers 14 and 15 had gradually tapered gage lengths such that their minimum width was 1.75 cm. Specimens numbered 13 through 23 were shot peened in the transition region beyond the test section into the grip tabs. All specimens were machined from sheared blanks, clamped in a stack between steel guides. They were likewise mechanically polished to a surface finish of about 38 μcm. Fabricating specimens this way reduced scatter caused by dimensional variations and avoided inadvertent rounding of otherwise square corners during the polishing operation.

Notched specimens had a planform similar to that of the smooth specimens with the exception that the test section contained a symmetrically placed right circular hole. The sheared blank size was nominally 27.94 cm by 12.70 cm, symmetrically tapering through a 2.54 cm radius into a test section 7.62 cm square that contained a centrally placed circular hole, nominally 1.27 cm diameter. These specimens were machined from sheared blanks in a stack in the manner of the smooth specimen. The hole was drilled 0.76 mm undersize, machined to its final size in steps of about 0.381 mm, and then honed to a finish of about 38 μcm. The final average diameter of the hole was 1.275 cm with an unbiased estimate of standard deviation of 0.0016 cm. The corresponding average value

of the theoretical stress concentration factor, K_t, has been determined, according to Howland[13], as 2.58 (for the net section). Both smooth and notched specimens were oriented along the grain (rolling direction) of the blanks. A total of six notched specimens and five smooth specimens were cut from each blank, numbered A125 through A130.

Because (as indicated by the experimental program of Table 1) specimens were to be loaded in compression as well as in tension, buckling guides were needed to provide lateral support. The buckling guides consisted of a stiff metallic plate element located symmetrically on both sides of the specimen, positioned by guide pins and nylon bushings. These plate elements were snugly clamped about the specimen such that the specimen could just move freely on the graphite bearing plates located between the specimen and the guide plate. The guides provided full lateral support to both specimen types over the surface between grips with the exception of access regions to install and support appropriate instrumentation. Modulus checks on the smooth specimens verified that the guides as installed in this program did not influence the test results. Figures 1(a) and 1(b) are photographs of the guides and specimens for the smooth and notched configurations, respectively.

APPARATUS AND PROCEDURE

Smooth Specimens

Data reported herein were derived from axially loaded specimens tested in two similar closed-loop servocontrolled electrohydraulic test systems. All testing was performed in strain control.

Strain was controlled over a 0.190-cm gage length using a clip-on extensometer calibrated to ASTM Class B_1. Strain was programmed to follow a sinusoidal waveform at frequencies ranging from 0.1 Hz to 30 Hz, depending on the amplitude of the control strain. The ability of the extensometer to operate over this range of frequencies was independently verified as a function of the strain amplitude prior to beginning the test program. To ensure that the temperature of the reduced section remained ambient in tests with either large strain amplitudes or higher frequencies, the frequency was chosen so that the

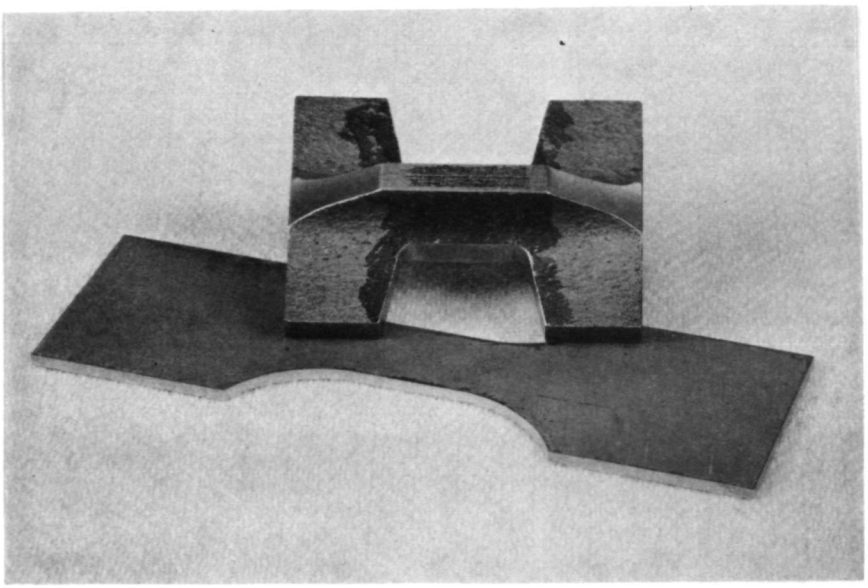

(a) Smooth specimen.

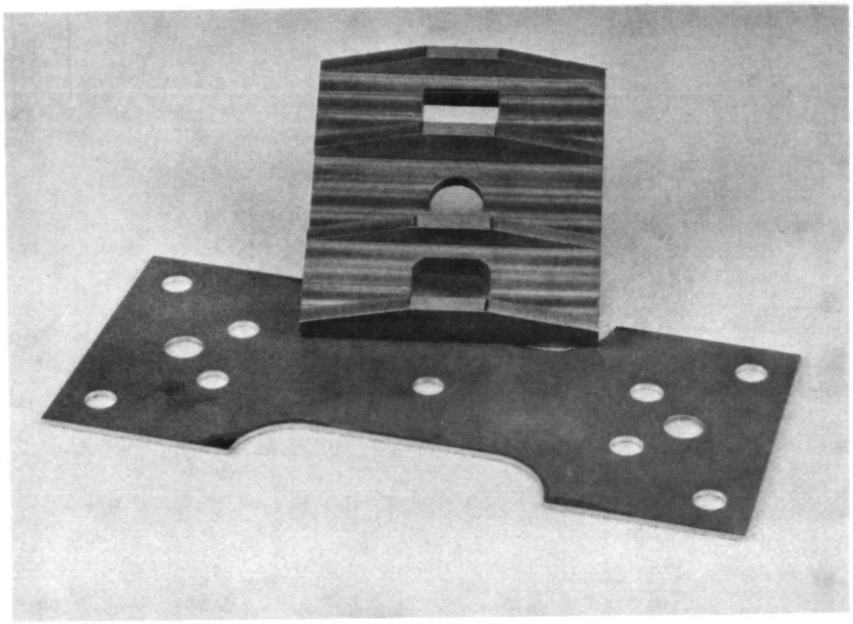

(b) Notched specimen.

Figure 1. – Smooth and notched specimens and the antibuckling guides.

indicated temperature (monitored via a thermocouple looped about and in contact with the shoulder) remained constant (within 3 K) during testing. Strain was controlled to within 1 percent of the programmed signal. The extensometer calibration was performed and verified several times during the test program.

Load was monitored in all tests using a commercially available load cell mounted in series with the specimen. Calibration of the load cell was performed prior to and verified once during the test program. The load cell was observed accurate and linear within 0.1 percent of the operating range used.

All specimens were gripped in a self-aligning hydraulic fixture which is designed to minimize specimen mounting stresses. Prior to commencing the test program, the alignment was adjusted to minimize bending strains, the adopted standard being bending strains less than 1 percent of the imposed axial strain for axial strains on the order of 0.5 percent. Figure 2(a) is a photograph of the overall test arrangement used, whereas Figure 2(b) is a close-up of the gripping, the specimen, the buckling guides, and the extensometer.

Monotonic and cyclic deformation response were recorded continuously during the first ten cycles and at logarithmic intervals thereafter on an X-Y recorder, while both load and strain were continuously recorded on a time-based high-speed strip chart recorder. Specimens were examined after separation to determine if the failure was representative of the bulk of the metal or if it initiated at some processing flaw or inclusion. No detailed metallography of the fractures was performed. All data reported herein were derived from test records in accordance with the ASTM Committee E09.08 draft of a tentative standard for fatigue testing practice.

Notched Specimens

All testing was performed in similar closed-loop electrohydraulic testing systems under axial load control via a load cell mounted in series with the specimen (this cell's accuracy is comparable to that used for smooth specimen testing). Load was programmed to follow a sinusoidal waveform at frequencies ranging from 0.01 Hz to 20 Hz. Load was controlled to within 1 percent of the program signal. Low frequencies were used early in the life in all tests over the period of the life during which local strains were measured, and throughout the life in specimens with notch root strains greater than the yield strain.

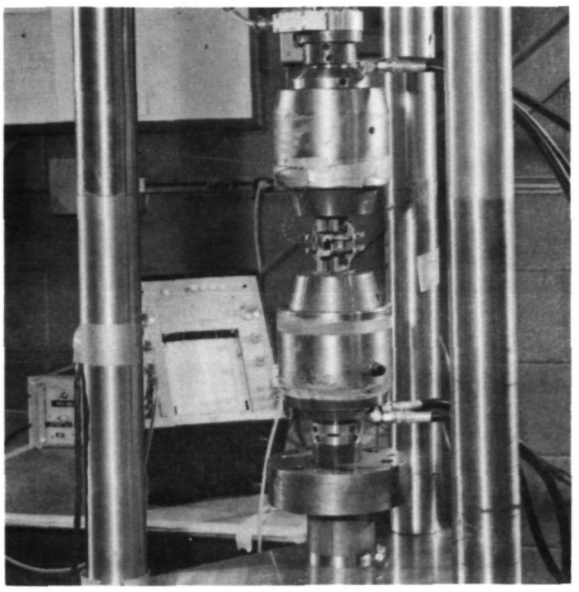

(a) Overall set-up.

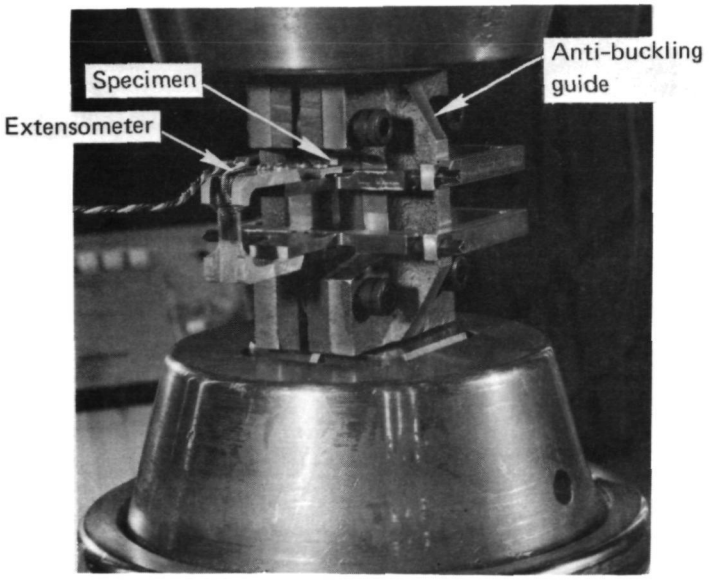

(b) The specimen and extensometry

Figure 2. — The smooth specimen test arrangement.

Higher frequencies were utilized in all other situations. All tests were started in tension, most under automatic control. Stroke was monitored in all tests. All specimens were gripped in a plate grip fixture adjusted for samples nominally 2.3 mm thick such that the load transfer was symmetric about the longitudinal and transverse center lines. The fixture transferred load through both friction and shear. Eccentricity was held less than 0.025 mm through periodic checks and adjustments. Figure 3(a) is a photograph of the overall test arrangement utilized in this study, whereas a close-up view of the specimen installed in the grip fixture is shown in Figure 3(b). The setup shown in part (b) of this figure was typical of that used for zero-tension (R = 0) testing; that shown in Figure 3(c) details the setup used for fully reversed (R = -1) loading.

As with the smooth specimens, records of the pertinent variables were made on X-Y recorders and strip chart recorders over the duration of the test. The relationship between applied load and notch root strain was recorded continuously over the first ten cycles on an X-Y recorder and thereafter at logarithmic intervals. These two variables were also recorded continuously on a time (cycle) base recorder along with stroke and the calibrated output from the eddy current device.

SPECIAL INSTRUMENTATION

Notch Root Extensometer

The history of notch root strain measurement is extensive. Early work focused on photoelastic models, the results being used primarily to validate values of K_t obtained from elasticity analysis and develop data regarding K_t in situations where analytic solutions were not available. Subsequently, use was made of optical/mechanical devices, again to evaluate K_t (see Reference 14). Later with the advent of new transducers, electromagnetic, resistive, and electro-mechanical devices have been employed in turn by a variety of authors[15,16] primarily in a study of notch root strain as a function of monotonically increasing load. Other authors have utilized a variety of optical techniques (developed for whole field displacement studies as compared to those above

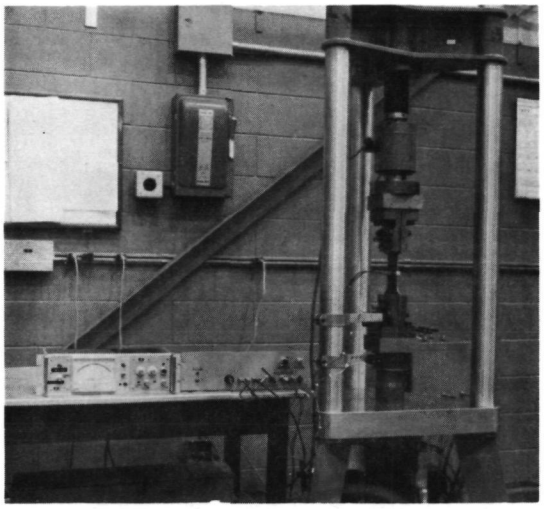

(a) Overall setup.

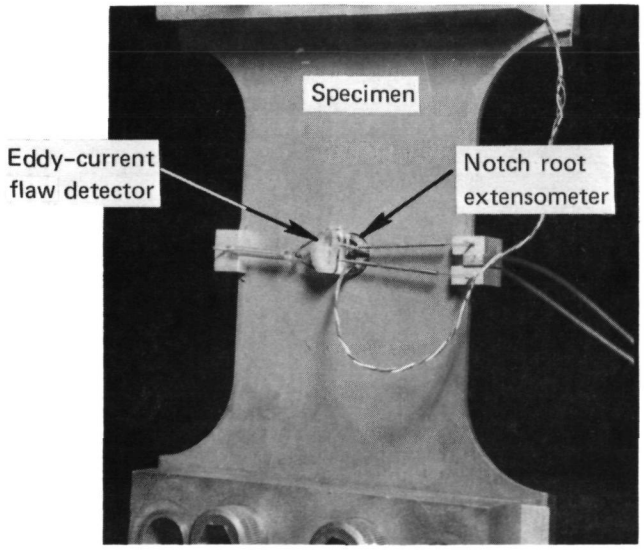

(b) The specimen setup for
zero tension cycling.

Figure 3. — The notched specimen test arrangement.

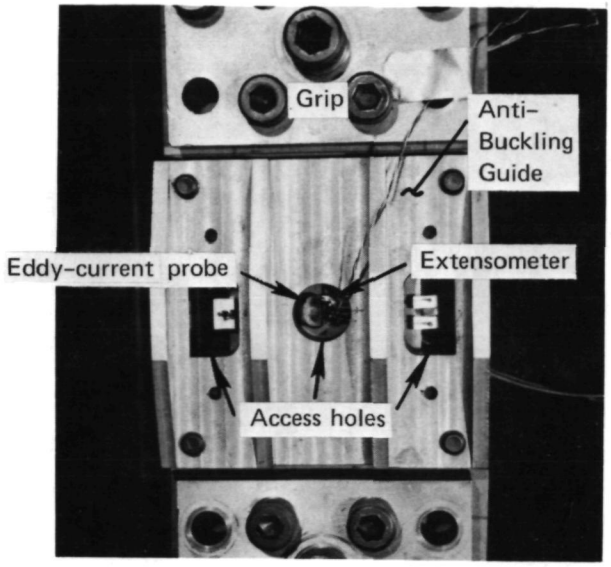

(c) The specimen setup for fully reversed cycling.

Figure 3. – (Concluded).

used for discrete measurement). Again, these studies examined primarily the case of monotonically increasing load.

Eventually, interest turned to fatigue problems and the attendant study of notch root strain under cyclic loads. Of the above techniques, only the electromechanical and resistive transducers are conveniently adapted to the continuous measurement of cyclic notch root strains. Griffith[15] was one of the first to perform such measurements, making use of an electromagnetic gage at the notch root. Subsequently, several authors have measured cyclic notch root strains, principally using electrical resistance strain gages in notched plate specimens and dimetrical extensometers in circumferentially notched bars. Crews and Hardrath[17] utilized both strain gages and a birefringent coating in their studies, the later technique being abandoned because of attendant difficulties. Because this study has avoided local biaxiality such as is encountered in circumferentially notched specimens through the use of a "thin" notched plate, strain gages appeared to be the logical choice to measure notch root strain. But, recent experience indicates that strain gages drift and undergo a calibration change under the action of cyclic inelastic straining[5]. Since a

goal of this program was to accurately measure notch root strain, an alternate transducer was chosen. The logical choice, based on the successful application of extensometers to measure cyclic strains in smooth specimens, was a notch root extensometer.

The design criteria for the notch root extensometer were: (1) to fit into a 1.25 cm diameter hole, sharing that space with a device to sense crack initiation, (2) have low knife edge forces to avoid crack initiation due to the instrumentation, (3) have a sensitivity adequate to measure accurately, with high precision, strains on the order of 0.10 percent. BCL designed and fabricated such a device, a photograph of which is shown in Figure 4(a). Note that the back of this device is aluminum (for flexibility), the arms are titanium (for stiffness) and the knife edges are a hardened steel. Calibration of the extensometer was accomplished using the jig shown in Figure 4(b)(also designed and fabricated at BCL). Observe in Figure 4(b) that both optical and mechanical calibration have been provided for. Prior to calibrating the extensometer, the mechanical micrometer (1 division equals 0.00005 in. (0.000127 cm)) and the filar micrometer (1 division equals 0.00004 in. (0.000102 cm)) were calibrated by an electromechanical device whose calibration is traceable to the National Bureau of Standards. Their calibration against this standard, which has a resolution on the order of 0.0000025 cm, indicated displacements on the order of 0.000015 cm could be repeatably imposed within $\pm$ 0.0000025 cm as measured using the mechanical and filar micrometers which form a part of the extensometer calibration jig. Calibration of the notch root extensometer was performed over the range of displacements anticipated in measuring notch root strains. Thus for the 0.127 cm gage length, maximum displacements on the order of 0.00254 cm (2 percent strain) were of interest. Consequently, the device was calibrated to give (1) 2 percent strain = 0.00254 cm displacement = 10 volts, and (2) 0.4 percent strain = 0.0005 cm displacement = 10 volts. For purposes of calibration, the excitation voltage to and the amplification of the output voltage from the full bridge on the flexible ligament of the extensometer was provided by a commercially available signal conditioner. After conditioning, the bridge output was fed to both a digital voltmeter and an X-Y plotter. Calibration indicated that the output of the extensometer was linear within 1 percent of the range when mechanical backlash in the calibration jig was accounted for. Available elasticity analysis for open hole sheet specimens [18] indicates the inaccuracy of this device due to its finite gage length is on

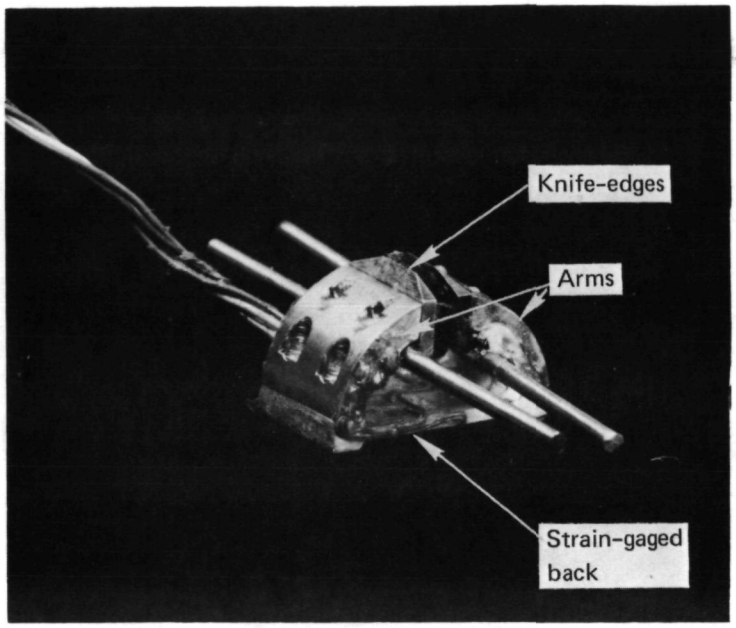

(a) The extensometer.

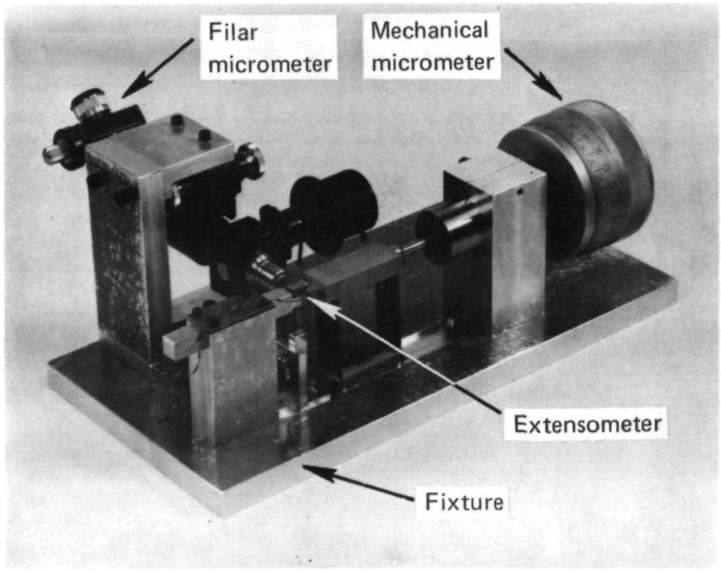

(b) The calibration jig.

Figure 4. – The notch root extensometer and calibration jig.

the order of -2 percent, so long as the strain field is elastic. The extent to which the magnitude of this error is influenced by inelastic action cannot be assessed without appropriate analytical data such as that reported later in the Analytical Aspects section. The extensometer was calibrated once before the experimental program began, twice during the program, and at the completion of the testing. No significant changes were observed.

Photographs of the notch root extensometer mounted on the specimen have been shown in Figures 3(b) and 3(c).

Crack Initiation Detection Device

While the history of crack initiation detection devices does not trace as far back as that of notch root strain measurement, the recent growth in nondestructive inspection (NDI) technology makes it as extensive. Let it suffice to state here that of the many indirect measurement tools available within the scope of NDI technology, those most useful in automated (for convenience and repeatability) crack initiation detection are the ultrasonic, acoustic emission, and eddy current techniques. Basically, these techniques compare current observations to some reference performence (calibration) standard in terms of some form of energy, the calibrated difference being electrically amplified, conditioned and output to some recording device. To meet the objectives of this program, the technology chosen had to be capable of detecting small cracks ($\ell_i \leq 0.1$ mm) in aluminum alloy sheet specimens containing a central notch 1.27 cm in diameter, laterally supported by buckling guides. Clearly, a technique which is locally sensitive is most appropriate. Consideration must also be given to accessibility of the specimen within the buckling guide sandwich and the fact that the notch will also contain the extensometer discussed earlier. In view of these requirements, BCL chose eddy current technology as a basis for automated crack initiation detection. This required the design of a transducer and the development of appropriate signal conditioning which possessed the necessary long-term stability (36 - 72 hours) needed to detect initiation in high-cycle (long-life) fatigue tests.

The transducer configuration and coil type were dictated by the experimental setup shown in Figure 3(c). Clearly, crack initiation at the notch root can

be best sensed by interrogating the confined region within an included angle of about 20 degrees about the transverse net section. Consequently, BCL developed a coil designed to interrogate this arc length to a depth of about 2.54 mm using eddy currents circulating in the material at the notch root. Upon crack initiation, this circulation would be perturbed and sensed as a change in the inductive reactance of the coil. The probe, a photograph of which is shown in Figure 5(a), was designed to seat the coil symmetrically about the specimen's thickness at a constant distance from the surface of the notch root. The probe was fixed to the specimen using a spring fixture as shown in Figure 3(b).

The excitation signal and signal conditioning were provided by a special unit developed by BCL. This unit (1) provided the excitation voltage for the coil as a 500 KHz sinusoidal wave, (2) permitted zero suppression of the output under reference zero conditions, (3) provided for calibration of the change of inductive reactance of the coil as a function of crack size, and (4) converted and amplified the change of the inductive reactance of the coil from the reference condition into a direct current voltage. Signal processing was developed such that the drift in the reference zero over the duration of the longest test (say 72 hours) was less than the minimum crack size detected in a short term test (threshold of about 0.003 cm). Actual drift observed in a bench test just prior to beginning the test program was about 0.005 cm over a 60-hour period. The drift was essentially uniform over that time period and had the sense of increasing crack size.

Calibration of the eddy current device was accomplished using the calibration plate shown in Figure 5(b). This plate contained plane front flaws developed by electrical discharge machining having measured lengths of 0.254 cm, 0.127 cm, 0.025 cm, 0.013 cm, and 0.025 mm. The holes from which these flaws were developed were drilled, reamed, and honed in the same manner as the notched specimens. They were made from a sample of the material used to make the test specimens. The results of this calibration indicate that crack length, ℓ, was an exponential function of the corresponding voltage, V, when the probe interrogated the region directly below the flaw (i.e., $\ell = 0.004 \exp 2.31V$, where ℓ has units of cm). However, when the flaw was not centrally located in the field of interrogation, the sensitivity of the device decreased and the calibration changed substantially. Under optimum conditions of probe placement, the threshold sensitivity of the device was a flaw of length 0.004 cm. Thus, assuming

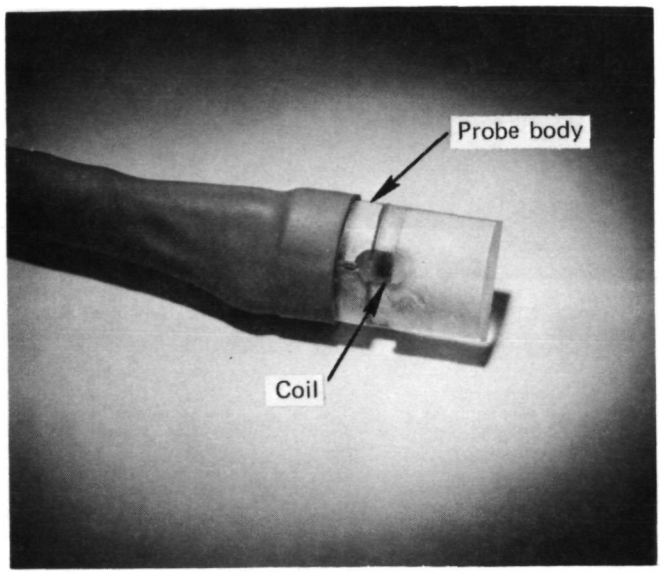

(a) The detection device.

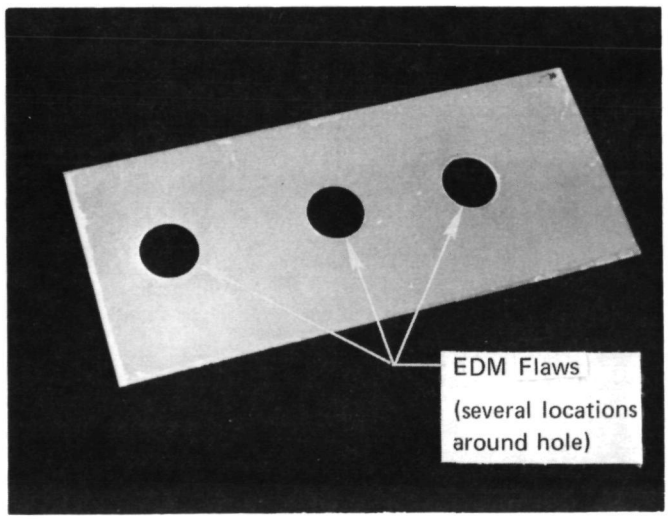

(b) The calibration standard.

Figure 5. – The crack initiation detection device and calibration standard.

the crack front is parallel to the initiating surface, the minimum detectable crack size was 0.004 cm. In addition to the use of the eddy current device, crack initiation was manually detected through visual checks using a 10 power microscope. Frequently, changes in specimen compliance were also utilized to infer initiation.

EXPERIMENTAL RESULTS

Raw Data

In this experimental study of the cyclic deformation and fatigue resistance of smooth specimens subjected to constant amplitude strain cycling, the corresponding load response and the number of cycles to cause specimen separation have been measured. Table 2 presents the results of this study in terms of the axial stress derived by dividing measured load by the net section area at the line of failure (perpendicular to the load axis) upon the first reversal and at the stable cyclic state[19], and cycles to failure for each of the control conditions. The most probably relative error (square root of the sum of the squares of contributing errors) in the controlled strain at the smallest strain level listed in Table 2 is $\pm$ 3.16 percent while that for the largest strain level is $\pm$ 1.41 percent. The corresponding relative errors in measured stress are $\pm$ 2.24 percent and $\pm$ percent, respectively.

The experimental program concerned with notched specimens likewise focused on both the cyclic deformation and fatigue resistance of the test specimen.

Locally, displacement over a small gage length at the notch root has been directly measured as a function of applied load cycles along with the initiation of a crack of a given size. With regard to the coordinate system defined in Figure 6, the $\theta\theta$ component of displacement at $\theta = 0, \pi$ has been measured over a chord length of 0.127 cm located symmetrically about the transverse net section. Values of this variable attained at the completion of the first reversal and after a stable cyclic state[19] is achieved are reported in Table 3 along with the corresponding number of cycles to crack initiation. Strains at this location are hereafter termed notch "root" strains. The most probable relative error in measured notch root strains is on the order of $\pm$ 3.16 percent

TABLE 2. — CYCLIC DEFORMATION AND FATIGUE LIFE DATA FOR THE 24S-T3 SHEET[a]

Specimen Number	Strain Range, Percent			Modulus[b], GPa	Stress, MPa			Life, Cycles	
	Δe^t	Δe^e	Δe^p	E	Tension S_{mx}	Range/2 $\Delta S/2$	Compression S_{mn}	Fracture N_f	Initiation[h] N_i
Monotonic Tension									
A127S1-S8	--	--	--	72.4	494.0	--	--	½	--
A129S1-S9	--	--	--	68.9	484.4	--	--	½	--
A125S1-S10	--	--	--	71.0	491.3	--	--	½	--
Fully Reversed									
A126S1-S2	3.00[c]	--	--	--	--	--	--	--	--
A125S1-S3	2.00	--	--	--	--	--	--	285	--
A128S1-S4	1.51	1.17	0.34	70.3	--	443.4	--	750[d]	695
A126S1-S5	3.06	1.38	1.68	68.2	--	493.3	--	145	127
A127S1-S6	1.02	1.00	0.02	71.0	--	362.4	--	7,195[e]	6,871
A127S1-S7	0.80	0.795	0.005	72.7	--	288.7	--	22,130	21,850
A129S1-S11	0.76	0.76	--	73.0	--	274.6	--	19,881[e]	19,625
A129S1-S12	0.76	0.76	--	73.0	--	274.2	--	26,400[e]	25,600
A125S1-S13[f]	0.76	0.76	--	72.3	--	274.9	--	29,196[e]	--
A129S1-S14[f]	0.76	0.76	--	71.7	--	272.8	--	29,192[e]	29,004
A120S1-S15[f,g]	0.58	0.58	--	70.3	--	206.7	--	170,800[e]	--
A128S1-S16[f,g]	0.495	0.495	--	69.6	--	172.3	--	604,900[e]	--
Mean Stress Tests[i]									
A128S1-S17[f]	--	--	--	--	289.4	--	0	315,940[e]	--
A130S1-S18[f]	0.50	--	--	68.2	377.6	--	32.4	30,090	30,013
A130S1-S19[f]	--	--	--	--	234.3	--	-167.8	113,910[e]	113,194
A130S1-S20[f]	1.50 to 0.57	0.92	0.01	69.6	406.5	--	-250.1	4,503[e]	3,721
A130S1-S21[f]	1.25 to 1.74	0.49	--	67.5	379.6	--	59.3	14,173[e]	12,500
A130S1-S22[f]	--	--	--	--	248.0	--	0	--	650,000[j]
A130S1-S23[f]	1.33 to 2.00	0.67	--	68.2	403.1	--	-54.4	10,841[e]	10,794

(a) Supplied by NASA Langley Research Center.
(b) Modulus for cyclic tests is for stable loop.
(c) Buckled.
(d) Crack initiation at extensometer knife-edge contact location.
(e) Broke at radius.
(f) Test section transition radius shot-peened.
(g) Test section tapered about center line.
(h) Life listed is for a 5 percent tension load drop; approximately a 5 percent loss in tension resisting area or a crack 0.9 mm long.
(i) Strain limits listed are the maximum and minimum values used to develop the mean stress in these mean strain controlled tests. Stress values reported correspond to stable response (there was little transient action so that these values are comparable to those developed on the first reversal).
(j) Test suspended, no failure.

TABLE 3. – RAW DATA DEVELOPED FROM NOTCHED PLATE EXPERIMENTS

Specimen Number	Control Condition: Fully Reversed ΔS/2, MPa	Control Condition: Zero[a] Tension S_{mx}, MPa	Local Strain: First Reversal Δε/2, %	Local Strain: Stable[f] Δε/2, %	K_t[g]	Crack Initiation[h]: Eddy Current: Cycles	Eddy Current: Length, cm	Visual: Cycles	Visual: Length, cm	Compliance[i]: Cycles	Cycles to Failure
A130S1-N1	Set-Up Specimen		Varies		--	--	--	--	--	--	--
A129S1-N2	--	Monotonic Tension	(e)	--	2.45	--	--	--	--	--	--
A128S1-N3	206.0	--	0.98	0.965	--	795	0.006	795	0.079	--	1,090[i]
A128S1-N6	168.1	--	--	1.02	--	630	0.003	--	--	670	800
A129S1-N5	239.1	--	--	1.015	2.72	--	--	--	--	475	689
A125S1-N6	240.5	--	1.16[d]	0.98	2.52	250	0.007	336	0.25	320	468
A125S1-N7	275.6	--	1.50[d]	1.25	2.49	--	--	282	0.079	270	349
A125S1-N8	137.8	--	0.52	0.52	2.50	13,200	0.003	--	--	17,500	21,455
A125S1-N9	103.4	--	0.30	0.30	2.98	--	--	110,000[m] 126,000	-- 0.76	--	135,600
A125S1-N10	172.3	--	--	0.60	--	--	--	3,347	0.079	3,600	4,238
A125S1-N11	137.8	--	0.51	0.51	2.53	12,900	0.003	--	--	17,000	21,219
A127S1-N12	103.4	--	0.36	0.36	2.55	--	--	111,000	0.079	--	134,300
A126S1-N13	86.1	--	0.28	0.28	2.44	--	--	--	--	384,000	411,400
A126S1-N14	68.9	--	0.26	0.26	2.46	--	--	<7,300,000	--	--	(j)
A127S1-N15	--	241.2	0.96[k]	0.40	2.76	20,000	0.10	--	--	20,400	21,484
A127S1-N16	--	275.6	1.10[k]	0.51	2.52	7,050[m] --	0.002 0.02	-- --	-- <0.05	-- 8,650	9,062
A127S1-N17	--	310.1	1.70[k]	0.53	2.51	3,667[m] --	0.002 0.03	-- --	-- 0.06	-- 4,800	5,000
A127S1-N18	--	206.7	0.80[k]	0.35	2.54	--	--	35,000	0.06	--	39,300
A127S1-N19	--	172.3	0.56[k]	0.28	2.54	50,000	--	--	--	48,000	56,323
A126S1-N20	Sample Inadvertantly Overloaded; Beyond Gross Section Yield										
A127S1-N21	--	137.8	0.507[k]	0.25	--	--	--	141,200	0.165	139,000	150,918
A129S1-N22	--	103.4	0.38[k]	0.19	2.60	--	--	<7,000,000	--	--	(j)
A126S1-N23	--	120.6	0.47[k]	0.235	2.57	--	--	--	--	344,500	382,720
A126S1-N24	--	172.3	(e)	--	--	--	--	--	--	48,500	71,650
A128S1-N25	--	137.8	(e)	--	--	--	--	243,000	0.95	222,550	255,500
A128S1-N26	--	120.6	(e)	--	--	--	--	--	--	175,560	221,360
A126S1-N27	75.8	--	0.27[k]	0.27	2.44	--	--	--	--	1,229,200	1,257,900
A128S1-N28	--	117.1	(e)	--	--	--	--	700,290	0.09	700,290	764,450

(a) Nominally zero load, the minimum stress in these tests was kept slightly positive (tension).

(b) Previous history in zero tension loading at S_{mx} = 110.2 MPa for 7.2 x 10^6 cycles; no evidence of cracking at 10X during inspection with a microscope. Present test started after cycle counter had been set to zero; test at S_{mx} = 110.2 MPa is considered a runout.

(c) Extensometer removed at 5 percent strain.

(d) Gross section cyclic creep evident in stroke response; stabilizes after about 10 cycles for N6 and 20 cycles for N7. Response manifest itself at notch root as a strain range with decreasing mean and amplitude.

(e) Notch root not instrumented.

(f) Value reported is one half the observed range.

(g) Experimentally observed value, computed from the product of measured elastic strain and the modulus of elasticity divided by the corresponding stress, for the first reversal of loading (tension loading portion).

(h) Shortest size observed for each of the three methods; when blank, the crack size is unknown. Note the shortest size is used to define initiation throughout this report. Eddy current size is based on the calibration for ideal crack location and orientation (see text); actual size may be larger.

(i) Crack initiation occurred first under a knife edge at 600 cycles; initiation under the eddy current probe followed at 795 cycles, crack growth was somewhat assymetric.

(j) Broke in grip, microscopic study indicates the presence of an extensive network of branched cracks on all 4 surfaces at the notch root. These cracks are evident at 20X leading from the root, the branching is evident above 60X. In the context of an initiation criterion of 0.1 mm, these cracks would be said to have initiated (see text).

(k) Peak strain on first reversal.

(l) Based on observations of ram stroke history.

(m) Brace brackets results for both roots of the notch.

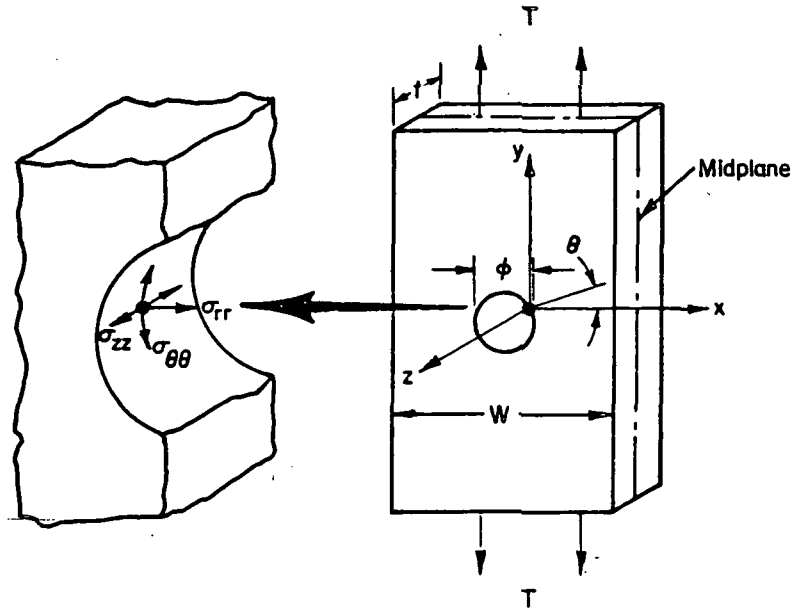

Figure 6. – Coordinate system for notched plate specimen.

over the range of notch root strains measured in this program. In general, the extensometer performed well and possessed adequate sensitivity without being so stiff as to require high force transfer at the interface between the knife edges and the notch root. Consequently, crack initiation occurred between the knife edges in all but one test, as noted in Table 3. In a few tests, the extensometer was observed to periodically make contact with the eddy current crack initiation device causing a drift in both signals. This continued until the devices were moved to provide clearance. In such situations, the output from the extensometer on the first cycle has been omitted in Table 3. Overall, the extensometer met the objective of the program to accurately measure cyclic inelastic notch root strains, free of zero drift.

Crack initiation is reported in Table 3 in some instances in terms of three means of detection. These are eddy current detection, specimen compliance change and visual detection. Of these, under ideal conditions (i.e., those that match the calibration), the eddy current device is most sensitive and repeatable. Of the remaining two, the visual approach is preferred to the compliance change for sensitivity and ease in measurement, but not for repeatability.

While under ideal conditions the eddy current device senses a crack of a given size with high repeatability, conditions in fatigue testing are less than ideal. There are several reasons. First, the device oscillates somewhat in response to all cyclic loadings which cause changes in the notch shape (attendant changes in the air gap between the probe and root occur that cause continuous changes in the reference state). Second, the fatigue crack seldom (if ever) initiates directly under the coil so that calibration of its output by the use of standard crack sizes (and shapes) is academic. Third, while the geometries of fatigue cracks in given specimen geometry may be similar, the corner crack shape and range of aspect ratios encountered in tests are difficult to simulate in calibration standards. Consequently, the absolute bench calibration against some reference standard is arbitrary in practical applications. The previously quoted threshold crack size is thus not the crack size at initiation indicated by the eddy current device. Indeed, because of any one of the above three reasons, the calibration of the device cannot be fixed in a practical sense without prohibitive cost. In cases where data are available for comparison purposes, the crack sizes derived from the eddy current calibration are smaller than the corresponding visual value by as much as a factor of 10. The device therefore, can only be used as a relative indicator of initiation. The crack size corresponding to this indication is less than 0.8 mm, a value somewhat larger than that desired in the context of the program's objectives.

Nominally, both deformation and life have also been measured as a function of the applied load cycling. Nominal deformation has been assessed in terms of the ram stroke (proportional to the nominal axial displacement of the gage section of the notched plate) while life has been directly measured in terms of the number of cycles to separation of the specimen into two pieces. Ram stroke has been used to assess the extent to which nominal cyclic creep has occurred (see note (d), Table 3) and to infer (indirectly measure) crack initiation as detailed in the previous paragraphs and in Table 3. Because stroke is an indirect measure of these events, direct stroke measurements are not reported. Instead, only the related observation is noted.

Certain of the data listed in Tables 2 and 3 are graphically presented in Figures 7(a) to 7(c) for the smooth specimens and Figures 8(a) to 8(d) for the notched specimens. Figure 7(a) presents the monotonic and stable cyclic deformation response while part (b) presents the stress response as a function of

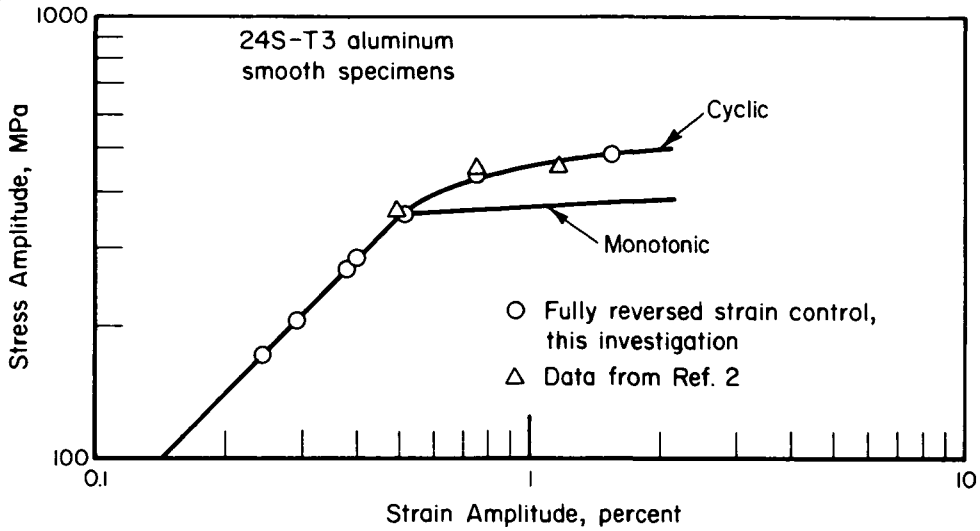

(a) Cyclic stress-strain response.

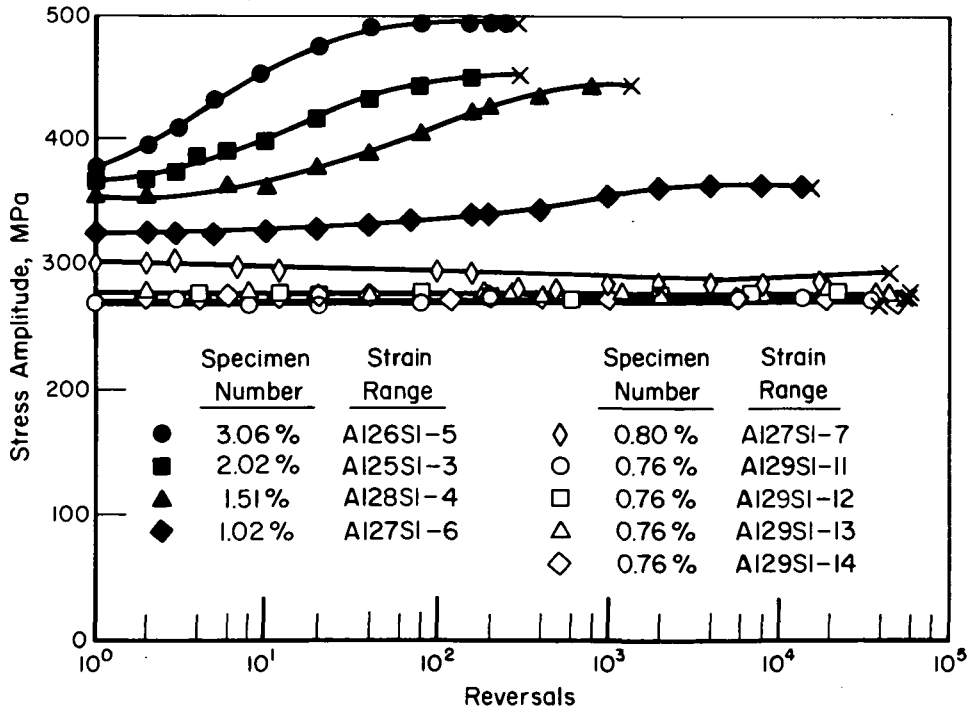

(b) Stress response as a function of cycles.

Figure 7. – Cyclic deformation response and fatigue resistance of 24S-T3 aluminum sheet material (fully reversed strain control).

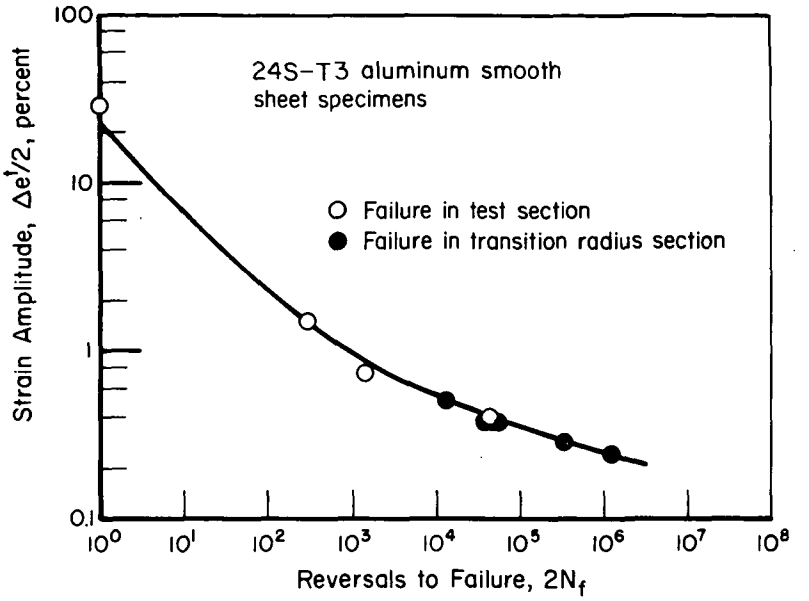

(c) Strain-life behavior.

Figure 7. — (Concluded).

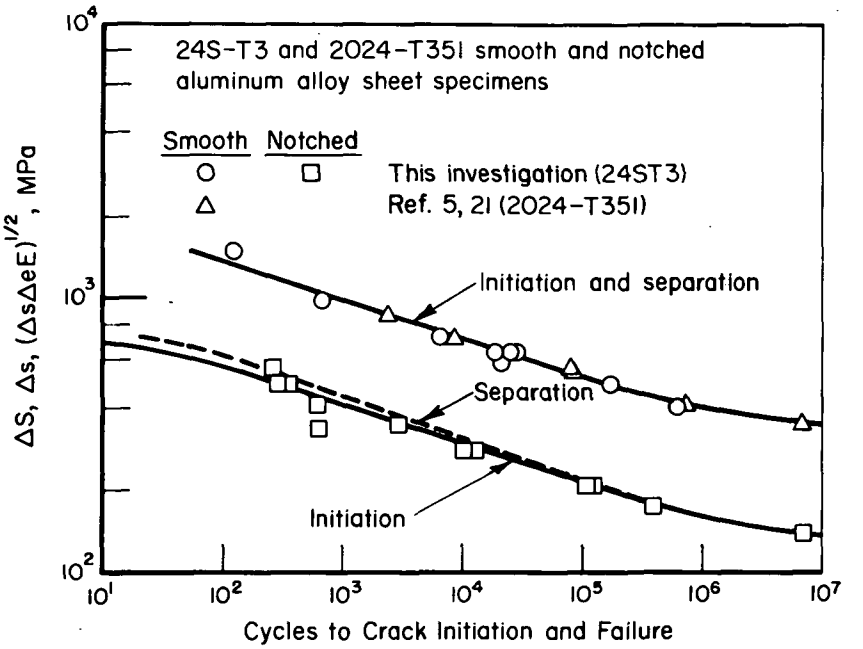

(a) Stress-life behavior for fully reversed load cycling.

Figure 8. — Cyclic deformation response and fatigue resistance of notched 24S-T3 aluminum sheet specimens under fully reversed load cycling.

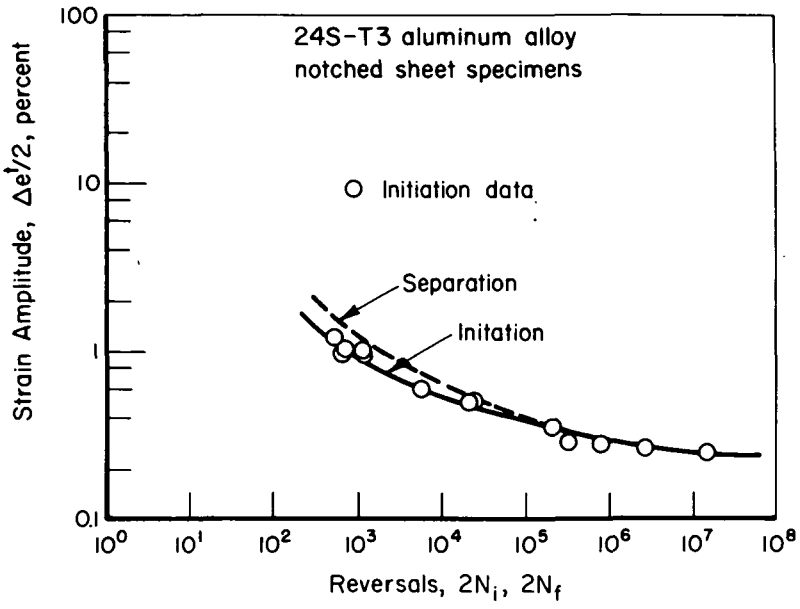

(b) Local strain-life behavior for fully reversed load cycling.

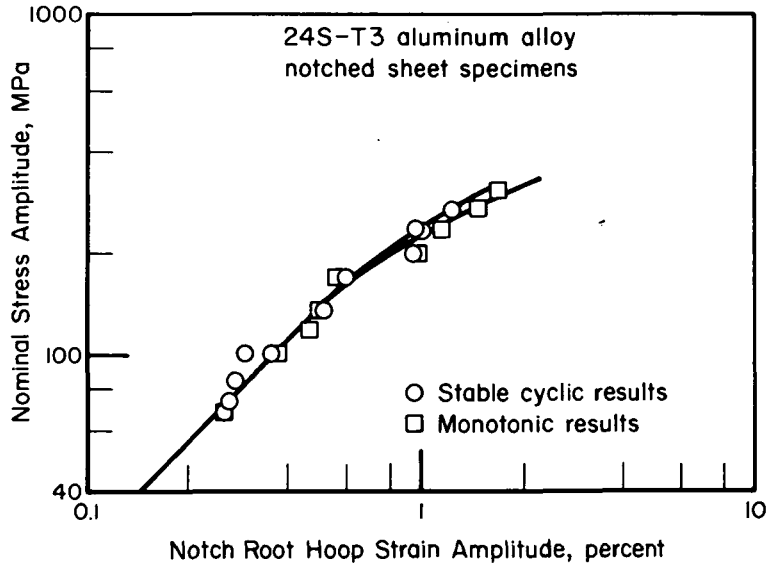

(c) Nominal stress-local strain response.

Figure 8. – (Continued).

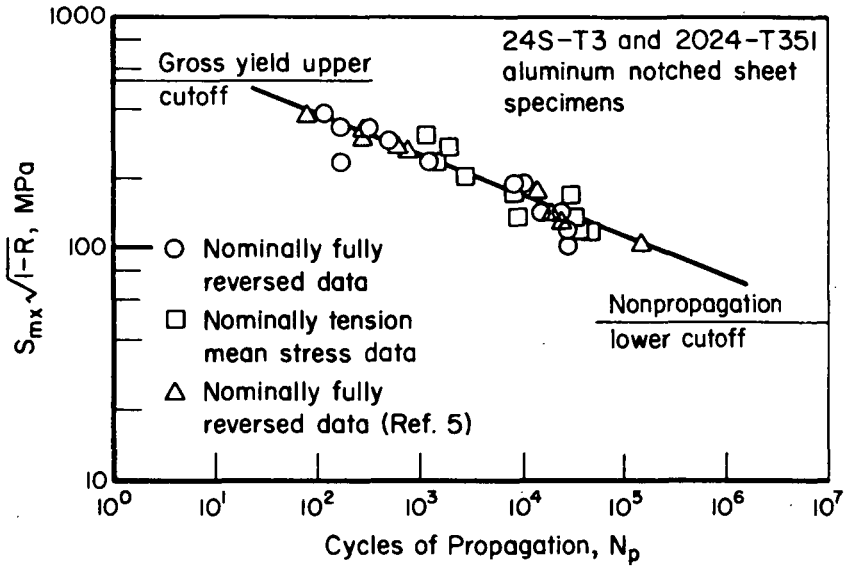

(d) Crack propagation period as a function of nominal stress.

Figure 8. – (Concluded).

strain reversals. Part (c) presents the fatigue resistance of the material in terms of strain amplitude and life to failure (separation). Figures 8(a) and 8(b), respectively, present the fatigue resistance of the notched specimen in terms of the nominal response on coordinates of stress amplitude and life and the local response on coordinates of notch root strain amplitude and life. Note that life is characterized in terms of both cycles to crack initiation and fracture for the notched specimens. Figure 8(c) characterizes the deformation response of the notched specimen on coordinates of nominal stress amplitude and notch root strain amplitude. Note the coordinates of this figure correspond to those of Figure 7(a). Finally, Figure 8(d) depicts the observed relationship between the crack propagation period (N_f-N_i) and nominal stress expressed as a function of the maximum stress and stress ratio[20].

In each of Figures 7 and 8, data developed from this program are shown as open circles for fully reversed data and open squares for tension mean stress data. In several instances, data developed in this program are presented along with corresponding available data from the literature[2,5,21] for purposes of comparison. These data are represented by triangular symbols.

Derived Data

As evident in Table 2, smooth specimen tests at lower strain levels terminated in failures outside the gage length at the transition radius into the grip tabs. While such failures are usually avoidable through the use of specimen geometries with continuous curvature in the test section, these specimen geometries preclude gradient-free strain control as desired in this program. This fact, coupled with past extensive experience which showed out-of-gage-length failures[9] even with such a geometry for the material used in this program, suggested the use of a uniform test section geometry with subsequent correction (if necessary) for the notch effect to derive unnotched (smooth) specimen fatigue life data. Examination of the raw data (Table 2) shows that in all but one case, out-of-gage-length failures occurred at test levels that gave rise to essentially elastic nominal stress-strain response. Derivation of smooth specimen fatigue resistance from the raw data, therefore, follows by adjusting the nominal stress (and strain) to correspond to that acting at the toe of the transition radii. (That is by multiplying the nominal value by the corresponding value of the theoretical stress concentration factor.)

With reference to the smooth specimen geometry at the transition section, one can determine K_t in terms of the characteristic nondimensional parameters - the ratio of the step size to the transition radius, h/r, and the ratio of the transition radius to the net width, r/d, whose values for the current geometry are respectively, 0.59 and 1.43. Information on values of K_t at large values of r/d is scarce. None could be found for the particular value of h/r of interest. Values could, however, be found at values of h/r of 1.0 and 0.5 (which bound the value of interest) at values of r/d up to 1.0, as shown in Figure 9. Extrapolating these data to r/d > 1.5 suggests that K_t for the geometry of interest is bounded by values of 1.16 and 1.145 (see Figure 9). For the present case of h/r equal to 0.59, K_t will be taken as 1.15. Accordingly, the elastic strain-life line of Figure 7(c) will shift up to follow the adjusted data as shown in Figure 10(a). Note that after this adjustment, these data correspond closely with that reported in the literature. As with Figure 7(c), smooth specimen life has again been shown in terms of life-to-specimen separation.

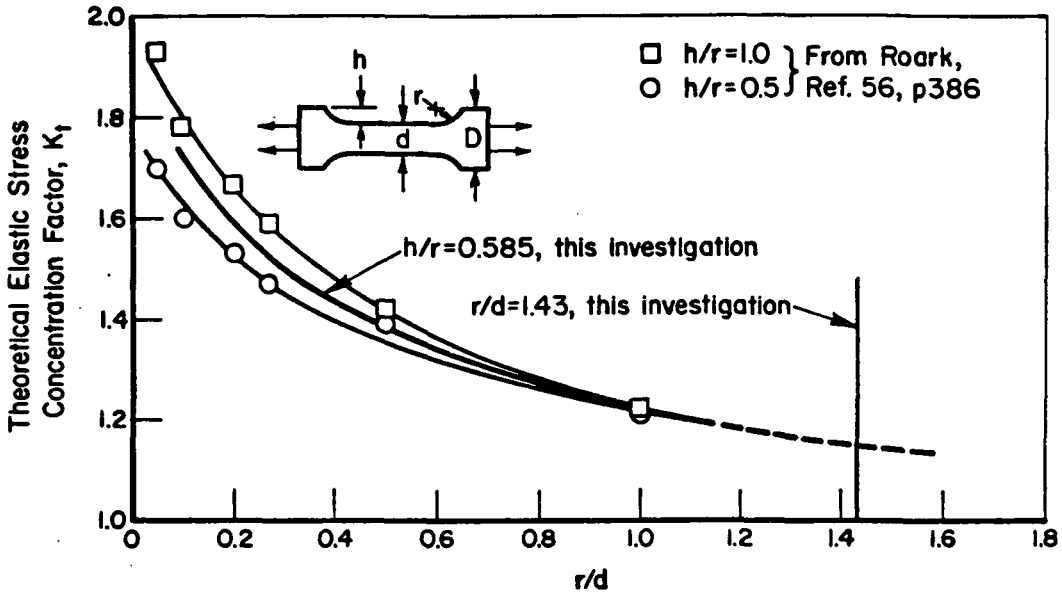

Figure 9. – Elastic stress concentration factor as a function of smooth specimen shoulder-fillet geometry.

Measures of life-to-crack initiation for the smooth specimen derived indirectly from specimen compliance are also plotted in Figure 10(a). The curve denoted as "initiation" has been derived by back extrapolation of the asymmetric compliance change associated with the area loss due to the propagation of an initiated fatigue crack. Since asymmetric compliance changes that are less than 5 percent could be consistently resolved, the crack size associated with this definition is on the order of 1 mm. (Visual checks and correlation with the crack size are not available because the crack was blocked from view by the buckling guides.)

The strain-life data shown in Figure 10(a) characterize only the fatigue resistance of the material under fully reversed strain control. To compare these data with that of the material subjected to conditions other than fully reversed requires the introduction of a damage parameter that embodies the influence of mean stress on fatigue resistance. For present purposes, the form $s_{mx}\,\Delta e/2$ will be used. This form is a special case of a more general energy-based damage parameter[22]. It has the same general form as the Walker[23] parameter and is identical to the form hypothesized by Smith, et al[20]. According to this parameter, the damage-life relationship for the smooth specimen data

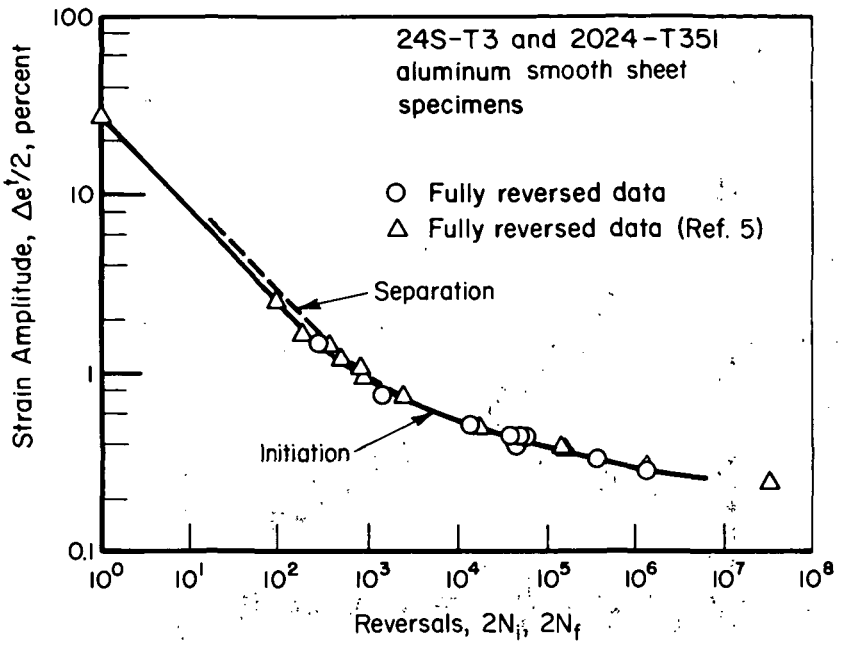

(a) Fully reversed results on strain-life coordinates.

Figure 10. — Fatigue resistance of 24S-T3 aluminum sheet material - adjusted based on failure location.

developed in this program is as shown in Figure 10(b), for both definitions of life (i.e., initiation and fracture).

Data have also been derived that characterize the stress response at the notch root. Here notch root stress has been defined as the stress corresponding to that obtained assuming uniaxial notch root stress-strain response which follows that depicted in Figures 7(a) and (b). In cases where the external loading is fully reversed, the maximum stress corresponds to the fully reversed stable stress. In cases where the external loading is not fully reversed, the stress reported corresponds to that obtained on the first reversal of loading. In the latter case, it has been assumed that the maximum stress attained during the life is equal to that developed during the first reversal. This assumption is consistent with the observations of the material's transient response which showed little change in maximum stress, apparently due to the action of competing transient mechanisms - hardening to increase the maximum stress and relaxation to decrease the maximum stress. Note, too, that the plastic strain range is small so that there is little driving force for such transient action. Figure 10(c) presents data developed from notched specimen testing on coordinates of life and the product of measured notch root strain and the derived maximum stress.

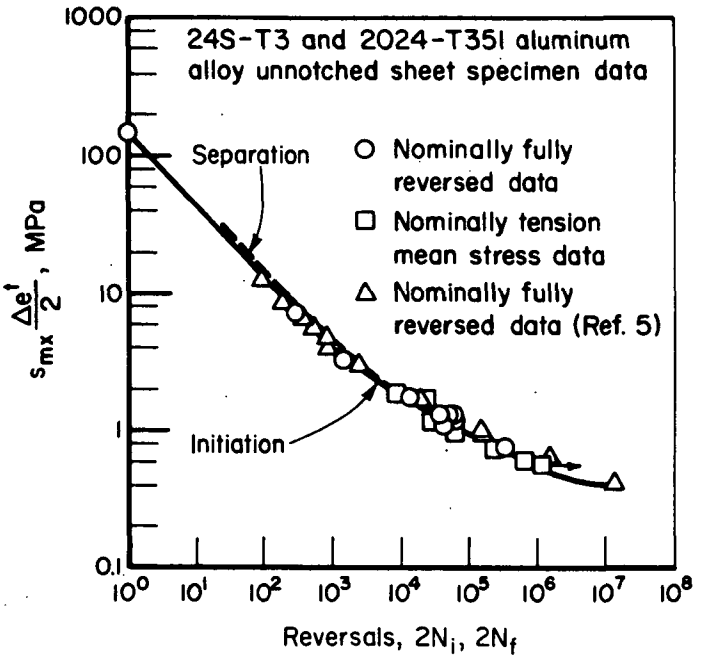

(b) Mean stress and fully reversed results on $s_{mx} \cdot \Delta e^t/2$-life coordinates for smooth specimens.

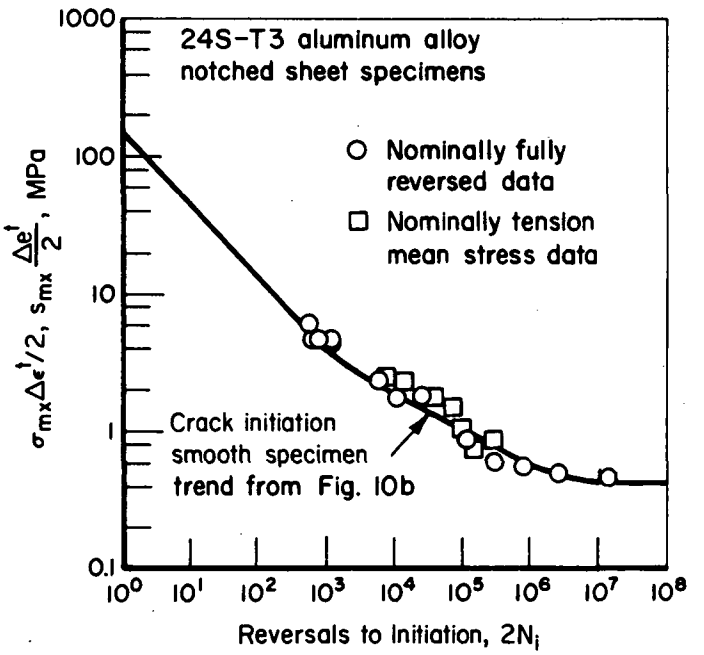

(c) Mean stress and fully reversed results on $\sigma_{mx} \cdot \Delta e^t/2$-life coordinates for notched specimens.

Figure 10. – (Concluded).

Data presented in Figure 10(c) for notched specimens correspond to those for smooth specimens shown in part (b) of this same figure. Likewise, data shown in part (a) of this figure for smooth specimens correspond with that measured at notch roots, as shown previously in Figure 8(b). Direct comparisons of these corresponding smooth and notch root deformation-life relationships are shown in Figure 11(a) on a strain basis and in Figure 11(b) on the basis of the product of maximum stress and strain amplitude.

SUMMARY AND DISCUSSION OF EXPERIMENTAL ASPECTS

This section has detailed the experimental aspects of this combined experimental/analytical investigation of an improved method of consolidating fatigue life data. The objective of the experimental program was to develop a complete internally consistent data set with direct measurements of all key parameters, including crack initiation and strain response at notch roots. These data will be discussed here in regard to issues on which they bear directly. They will subsequently be used to assess the validity of the various analytical models developed in the ensuing section.

Consider first a discussion of the cyclic deformation and fatigue life behavior of smooth samples of the test material. With reference to Figures 7(a) and 7(b), note that the material exhibits a cycle dependent hardening response that occurs at high rates very early in life under fully reversed constant amplitude strain controlled cycling. Rapid transient hardening at inelastic strain amplitude parallels that observed in previous studies of this class of aluminum alloy[1,4,5]. Present studies of mean stress relaxation in the presence of such transient hardening indicate that, while hardening reduces the propensity for mean stress relaxation (because of attendant decreases in the component of plastic strain), there is little net change in the maximum stress (elastic component of strain). With regard to the fatigue resistance of this aluminum alloy, shown in Figure 10(a), comparison of the data developed in this program shown as open circles with that reported in the literature[5] shown as open triangles indicates a close correspondence for strain-controlled fully reversed data, over the entire life range. As expected, this same close correspondence is evident when these same data are compared on the basis of the damage parameter, $s_{mx}\Delta e^t/2$, as shown in Figure 10(b). Note from each part

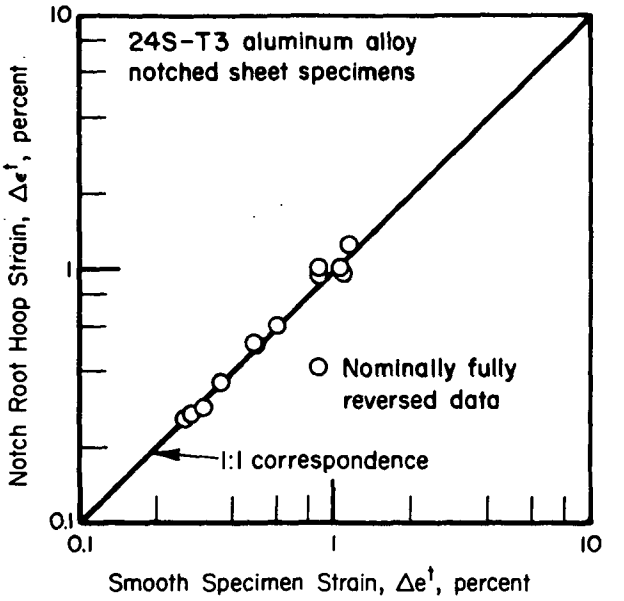

(a) Fully reversed data.

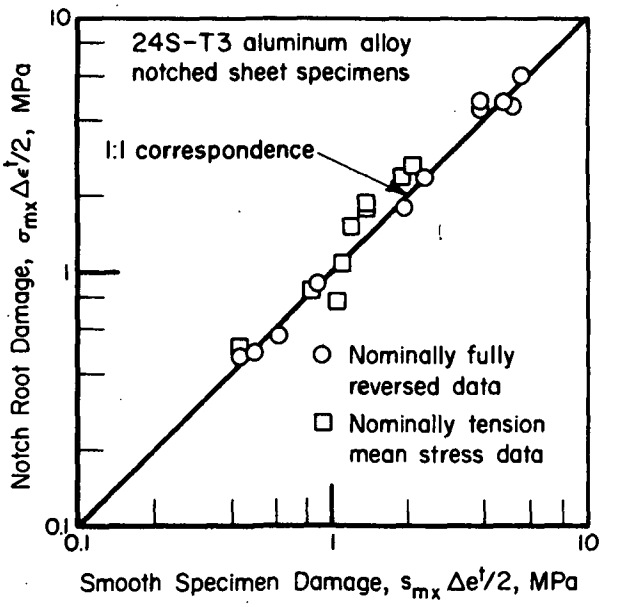

(b) Fully reversed and local mean stress data.

Figure 11. – Comparison of smooth specimen and notch root fatigue life to crack initiation resistance at corresponding lives.

of Figure 10 that the life-to-crack initiation at lives to initiation beyond 10^4 cycles is greater than 95 percent of the separation life, while beyond 10^5 cycles, the corresponding fraction is on the order of 100 percent of the total life. Recall that the maximum crack size is on the order of 1 mm for this compliance-based definition of initiation.

Consider now results for the notched specimen. With reference of the nominal stress-life behavior shown in Figure 8(a), note the characteristic sigmoidal shape of this relationship. Particularly note that regardless of the definition of failure, long life data for fully reversed load cycling lie at a stress level corresponding to the smooth specimen value reduced by K_t. Note also that at increasingly higher stress levels, the period of crack propagation is in relative increasing proportion to the total (separation) life. This behavior is replotted on an absolute basis in Figure 8(d) which shows the propagation period, N_p, increasing continuously as the net section stress decreases. The absolute period of propagation, of course, depends on the net section remaining after initiation, given that all other variables are held constant. Provided net section areas and planforms do not differ significantly, this dependence is only weak as evident in the close correspondence of the results for the two comparable geometries shown in Figure 8(d). Data from this investigation shown as open circles and squares compare closely with that from References 5 and 24, specimens for which were geometrically comparable to those of the present study.

In a practical sense, there are bounds to the power law relationship between applied stress and increasing crack propagation period shown in Figure 8(d). The upper bound corresponds with stress levels that induce gross yield in the notched specimen and the attendant cyclic creep. Clearly, the propagation of a fatigue crack and that due to a cyclic tensile instability are a result of different mechanisms and, therefore, would not be related. A lower bound for this power law relationship related to either the failure to form fatigue cracks or the failure to propagate fatigue cracks must also exist. With regard to the first of these, smooth specimen data indicate propagating cracks do not form at nominal stress levels below about 172 MPa. Consequently, cracks would not be expected to form at notch roots at fully reversed nominal stress levels below about 67 MPa (or in terms of the ordinate of Figure 8(d),

at 94.4 MPa). With regard to the latter of these, analysis indicates a lower bound of 48.6 MPa. This analysis utilized appropriate fracture mechanics technology, an assumed flaw size of 0.127 mm (corresponding closely to the program's desired crack initiation flaw size definition of 0.1 mm), and a threshold stress intensity for the material of interest of 13.78 MPa$\sqrt{m}$ [25]. Metallurgical examination of the initiation events at notch roots in specimens A126S1-N14 and A129S1-N22 shows evidence of initiation followed by branching, a behavior which reduces the driving force for propagation in proportion to n^2 (where n is the number of branches of equivalent length) [26]. In view of this observed branching, the appropriate lower bound is that for cracks which initiate but fail to propagate - 48.6 MPa.

There is yet another interesting feature of the initiation-propagation behavior of the notched specimens. Fractographic examination of these specimens showed regions of corner crack initiation that in every case reflected light much better than the surrounding regions of propagation. Such an appearance implies the rate of the process in this small corner crack region differs substantially from that in the adjoining material. Examination of the available records of crack initiation and subsequent growth obtained using the eddy current device (and in one case the extensometer) also bore evidence of this fact, the results showing either a very high rate of initial growth or a pop-in effect. In many cases, this initial corner flaw appeared symmetric about the corner with a length on the order of 0.8 mm.

Consider next measured notch root strain as a function of the applied nominal stress, results for which are shown in Figure 8(c) for both monotonic and stable cyclic loading. Note that while there is some scatter, the monotonic data indicate a local plastic strain component larger than that for the corresponding stable cyclic data at larger strain levels. This difference is probably due to the action of cyclic hardening in the metal in the notch root plastic zone. With reference to the measured values of K_t listed in Table 3, their computed mean value of 2.56 is represented in Figure 8(c) by a line with slope of unity which passes through the point (68.9 MPa, 0.00256). Both monotonic and stable cyclic relationships between nominal stress and notch root strain can be adequately characterized by power law equations for each of the elastic and plastic components of the total notch root strain. Thus, $\Delta\varepsilon^t$ =

$\Delta\varepsilon^e + \Delta\varepsilon^P$, so that $\Delta\varepsilon^t = K_t\Delta S/E + (\Delta S/K_2)^{1/n_2}$, where K_1 and n_1 are fitting paramaters. Such an equation provides the transformation between nominal stress and notch root strain needed later in the data consolidation. The value of K_t used in this equation (a best fit to all monotonic data) is 2.56. It compares very closely with the theoretical value of 2.58 and is greater than that expected in view of the -2 percent error due to the finite gage length of the extensometer.

Consider next the fatigue resistance of a generic element of material at the notch root, results for which are plotted in Figure 8(b) on coordinates of total strain and life to crack initiation. Note that these data follow the same characteristic shape as the corresponding smooth specimen data. Likewise, the trend of these data on damage-life coordinates follows that for the smooth specimens. Direct comparison of smooth and notched specimen data indicates similarity not only in the trend but also in the absolute fatigue resistances, as evident in parts (a) and (b) of Figure 11. With regard to the fully reversed data, note that the correspondence is almost exact, the mean value of the ratio of notch root strain to smooth specimen strain at the same life being 1.02 with a standard deviation of 0.073. This close correspondence, which has been observed in many other data sets[27,28], implies that equal deformation at critical locations in smooth and notched specimens gives rise to equal life-to-crack initiation. Results for the positive means stress tests plotted along with the corresponding fully reversed results in Figure 11(b) likewise implies equal damage gives equal life. However, the scatter is somewhat greater and the mean value increased slightly when the damage parameter is used as a basis for the comparison. Considering only fully reversed results, the mean is 1.08 as compared to 1.02 while the standard deviation is 0.135 as compared to 0.073. These differences are attributed to the spread in the data caused by the inclusion of a stress term in the comparison. When the positive mean stress data are included, the mean value is 1.10 with a standard deviation of 0.17, a result which suggests the mean stress damage parameter does not collapse these data as well as might be expected (cf the fully reversed case).

ANALYTICAL ASPECTS

BACKGROUND

As noted in the Introduction, the purpose of this study was to develop an improved method of data consolidation based on recently developed fatigue life prediction technology. This technology involves two basic steps: (1) the transformation of nominal stress into notch root stresses and strains, and (2) the assessment and accumulation of damage caused by these local stresses and strains. This section outlines the analytical determination of the first transformation and the marriage of the above two steps into a fatigue analysis procedure, examines the basic assumptions and limitations of this procedure, demonstrates the procedure, and finally discusses its adaptation for fatigue life data consolidation.

MECHANICS ANALYSIS TO DEVELOP THE NOMINAL STRESS-NOTCH ROOT STRAIN TRANSFORMATION

To accurately determine the stresses and strains at the notch root of the open hole notched plate specimen requires the solution of the corresponding boundary value problem. Several approaches are available whereby numerical solutions may be obtained.[29-32] Of these, only the finite element method, based on the incremental theory of plasticity[33], can accommodate effects such as transient cycle dependent[29] material deformation response and stress (and strain) redistribution in the inelastic region surrounding the notch root. Clearly, such effects significantly alter the stress-strain distribution at the notch root as compared to the results of deformation solutions.[34] Accordingly, the finite-element method (FEM) has been adopted. The essential features of this method are reviewed in the ensuing paragraphs.

Finite Element Formation

An explanation of the finite-element method, which is extensively used for structural analysis, can readily be found in literature.[35] It is based on the assumption that the deformation behavior of each subspace within a set

which represents a continuum can be approximated by a simple functional form. The potential energy of a solid under certain ideal conditions is given by

$$V = \int_{\text{Volume}} \int_{o}^{e_i} [s_i \, de_i + s_o \, de_i] \, dv - \int_{\text{Volume}} u_i B_i dv$$

$$- \int_{\text{Area}} u_i F_i dA \quad ,$$

where the first integral is the work done due to internal stresses, s_i and s_o; the second due to body forces, B_i; and the third that arising from surface tractions F_i. In this expression, e_i are the strain components of deformation, s_i the stress due to current deformations, s_o the initial stress in the structure, and u_i the displacement components. For a finite-element system, the volume and surface integrals appear as summations of integration over each subspace (element) of the body.

The constitutive relations between stresses and strains make the form of the strain energy expression quadratic in the displacement derivatives. Thence, variational calculus leads to a system of equations for the unknown displacements in terms of the stiffness, [k], of the structure and set of applied forces, {F}.

$$[k] \{u\} = \{F\} \quad ,$$

the system being dependent on the functional form chosen to represent the displacement field. Since the finite-element method is based on the theory of Hermitian matrix operators, the nonlinearity in the load-displacement character of the structure associated with plastic behavior is generally modeled through a series of piecewise linear segments.

The computer program ADINA[36] has been used to carry out the numerical computations for determining the stress-strain state and the displacements. The three-dimensional element contained in the program was used. This element belongs to the "serendipity" family, generally known as an isoparametric type. The interpolation function for the element formulation is a quadratic polynomial as shown in Figure 12(a) (from Reference 37). The program admits the

definition of a variable number of nodes (8 to 20) to describe an arbitrary element. Various options are available within the program for the representation of elastic-plastic material behavior. All of them are based on the assumption of small, infinitesimal strains. The material model chosen for this work assumes that the von Mises stress and the Prandtl-Ruess[33] flow rule control yield and plastic straining in the material. This flow rule postulates the proportionality between the plastic strain increment, de_{ij}, and the corresponding stress deviation, s'_{ij}, as given by

$$de_{ij} = s'_{ij}\, d\lambda \ .$$

The above equation leads to what is generally known as an incremental or flow theory of plasticity. Inherent in the use of such a theory is the path dependence that governs the final stress state in the body.

The response of the material subsequent to yield is subject also to the hardening rule chosen. For the present work, the isotropic hardening option was selected. Thus, it has been assumed that during plastic flow, the loading surface dilates uniformly about the origin in stress space and that the increment (or decrement) of stress is always in the direction normal to the yield surface at the point.

For each load increment, the stiffness matrix of the structure undergoes changes due to the change in the material constitutive law for the elements that are accumulating plastic strain. Hence, the system of equations needs to be resolved every time there is a change in the plastic field within the structure. Consequently, the load beyond that which causes initial yielding in the structure is broken into a finite number and applied successively to the structural model. This load step size has been chosen such that it is consistent with a prescribed error tolerance in order to ensure convergence of result, as detailed later.

In addition to the load incrementation and stiffness reformation involved in the incremental theory, the ADINA program makes a further attempt at achieving accuracy of solution through correction of the error in residual forces. The error is due to the dependence of the strain rate on the instantaneous value of the stress, necessitating an estimate of the strain rate based on past

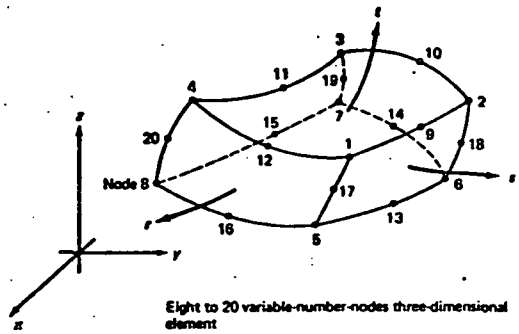

Eight to 20 variable-number-nodes three-dimensional element

$h_1 = g_1 - (g_9 + g_{12} + g_{17})/2$ $\quad h_5 = g_5 - (g_{13} + g_{16} + g_{17})/2$

$h_2 = g_2 - (g_9 + g_{10} + g_{18})/2$ $\quad h_6 = g_6 - (g_{13} + g_{14} + g_{18})/2$

$h_3 = g_3 - (g_{10} + g_{11} + g_{19})/2$ $\quad h_7 = g_7 - (g_{14} + g_{15} + g_{19})/2$

$h_4 = g_4 - (g_{11} + g_{12} + g_{20})/2$ $\quad h_8 = g_8 - (g_{15} + g_{16} + g_{20})/2$

$h_i = g_i$ for $i = 9, \ldots, 20$

$\beta_i = 0$ if node i is not included; otherwise,

$g_i = G(r, r_i)\, G(s, s_i)\, G(t, t_i)$

$G(\beta, \beta_i) = \frac{1}{2}(1 + \beta_i\beta)$ for $\beta_i = \pm 1$

$G(\beta, \beta_i) = (1 - \beta^2)$ for $\beta_i = 0$; $\beta = r, s, t$

Interpolation functions

(a) The element and interpolation functions.

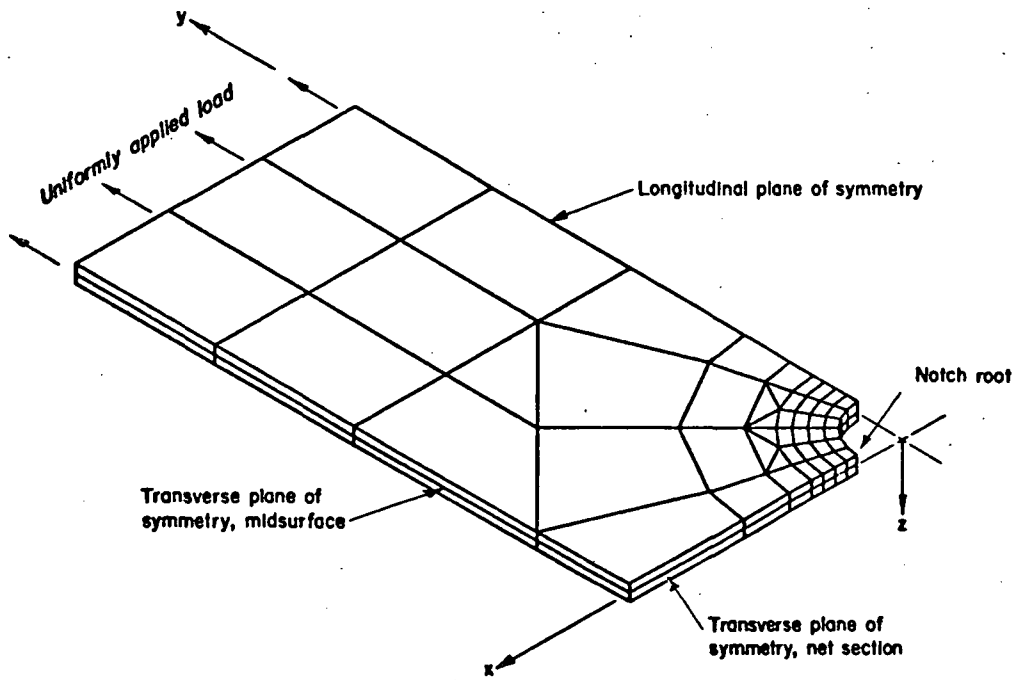

(b) The model.

Figure 12. — Model of the notched specimen for finite element analysis.

calculation and then computing the stress. Since the estimate for the strain rate cannot, in general, be expected to conform to the computed stress, iteration is required which suppresses the resulting error in the force equilibrium conditions at each nodal point. However, if stress reversal takes place in some element(s) for a certain load step, the switch controlling iteration to enforce residual load correction in the program must be shut off to prevent numerical instability due to oscillation between points on the load and unload branches

ADINA has an active column storage scheme for the master stiffness matrix and uses Gaussian elimination to decompose the matrix. The program also has the option of selective regeneration of element stiffnesses, thus limiting the computation during element stiffness generation to only those elements which are specified as being in the vicinity of the anticipated plastic zone.

The Model

The notched specimen was modeled through a set of three-dimensional finite elements. Due to the longitudinal and two transverse planes of symmetry in the specimen geometry and loading, only one-eighth of the specimen was modeled as shown in Figure 12(b). The finite-element mesh used consisted of 394 nodes and 48 elements. It was anticipated that plasticity would be confined to the region spanned by 12 of these elements. Hence, only the latter were declared as being capable of accumulating plastic strain, the maximum width of yielding from the edge of the hole being set at 0.3175 cm, based on past experience with such specimen geometries.[5] Subsequent computations substantiated this assumption for the level of loading imposed on the model. For the elements that were capable of exhibiting plasticity, a [3x3x3] Gaussian integration scheme was selected for use during the stiffness generation stage of the calculations. The other 36 elements which were declared to behave elastically were associated with a [2x2x2] scheme. The nodal spacing in the circumferential direction at the edge of the hole for the 90 degree arc length was 7.5 degrees. Appropriate symmetry conditions were applied to the nodal points on the planes $x = 0$, $y = 0$, and $z = 0$. Uniform load (stress) was applied perpendicular to the plane $y = 7.62$ cm, while the remaining two planes were

stress free. The load application sequence was tension-compression-tension with the amplitude in each case being held constant (to simulate constant amplitude cycling). Computations were performed for several load (stress) amplitude levels ranging from 1.1 to 1.5 times the load that initiated yield in the finite element model, as noted in Table 4.

The Young's modulus and elastic Poisson's ratio for the material were chosen as 68.9×10^3 MPa and 0.3, respectively. The yield stress during the first loading (tension) sequence was assumed to be 358 MPa and the tangent modulus E_t was 7.84×10^3 MPa. After the first load reversal, the yield value was changed to 413 MPa (at the zero load position) in order to simulate the cyclic hardening exhibited by the material. The tangent modulus was also modified to be 1.39×10^3 MPa at this point. The error tolerance parameter for performing residual load correction was set at 0.001, where the convergence measure is the difference between the Euclidean norms of the system displacement vector at successive cycles of iteration.

Results - Comparison with Experimental Data - Discussion

The complete raw results of the application of the finite-element method to the analysis of the stress-strain distribution at the notch root are too extensive to tabulate or graphically present in this report. Furthermore, they pertain to the response at integration points within the volume of the elements of interest along the hole boundary rather than on the notch-free surface. Consequently, in general, only information obtained after raw data manipulation will be presented. Specifically, data obtained from a two-dimensional analytic extrapolation of the gradient of strain to the notch root will be presented and directly compared with experimental data. Data examined in this context will relate only to the strain associated with the maximum net section stress (load) applied to the notched specimen on any cycle. Additionally, the nominal stress-local strain response predicted over three reversals of load will be compared with that obtained experimentally during the first two reversals and during stable local strain response.

Consider first the results obtained at the extremes of the imposed nominal load histories, results for which are shown in Figure 13(a) for each of the

TABLE 4. DETAILS OF LOAD CASES STUDIED

Load Sequence: Tension Load ⟶ Full Reversal (Compression)[(a)] ⟶ Full Reversal (Tension)

P_y = Load initiating yield in finite element model; Corresponds to a nominal (net section) stress of 150.3 MPa

Case	Load Amplitude	Number of Load Steps		
		Tension ⟶	Compression ⟶	Tension
1	1.1 P_y	2	9	6
2	1.2 P_y	3	7	4
3	1.3 P_y	3	8	6
4	1.4 P_y	4	10	8
5	1.5 P_y	4	18	16

(a) In one case examined, this compression load was equal in magnitude to the initial tension load; in the second case examined, this load was taken as zero.

cases detailed in Table 4. Curves shown are for both the fully reversed and zero-tension cases for the monotonic loading and stable cyclic cases. Results for the initial loading correspond closely with that obtained experimentally as evident in part (b) of this Figure. Likewise, that obtained for the stable cyclic case exhibits an equally close correspondence with the experimental data [data shown in Figure 8(c)]. Results for the monotonic and stable cyclic states differ, the stable cyclic strain being somewhat less than the corresponding monotonic value indicating a strain redistribution due to transient inelastic action in the plastic zone around the notch root. Analytically, this cycle dependent transient action was simulated over the period of three reversals by declaring new material properties at zero load on the unloading (second) reversal (i.e., monotonic properties are replaced by stable cyclic properties). The attendant redistribution of stress and strain is finished after the completion of the second and third reversals (i.e., after reloading to maximum load). Note that for the zero-tension case, the analysis indicated elastic unloading and reloading on the second and third reversals, respectively, for peak stress less than 300 MPa.

Differences in the nominal stress-local strain transformation induced by changes in material response are illustrated in Figure 14 which show predicted

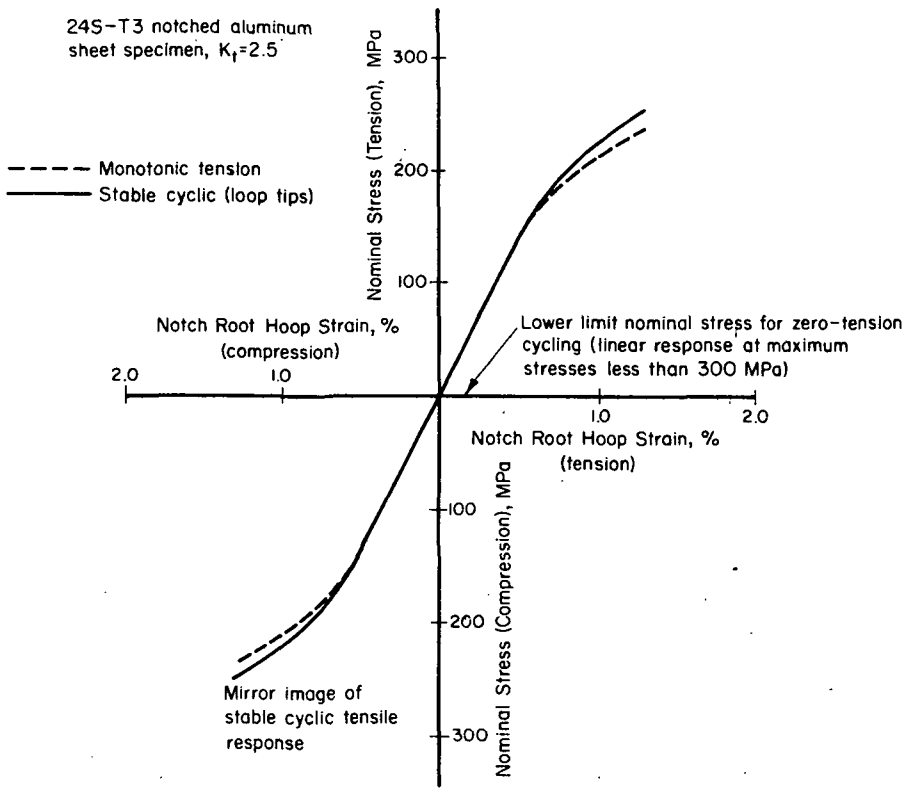

(a) Results of analysis.

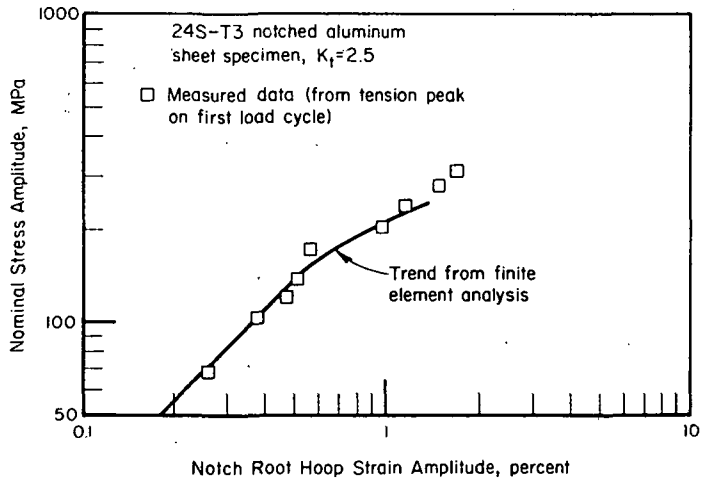

(b) Comparison of analytical and experimental results.

Figure 13. – Nominal stress-local strain response developed by finite element analysis.

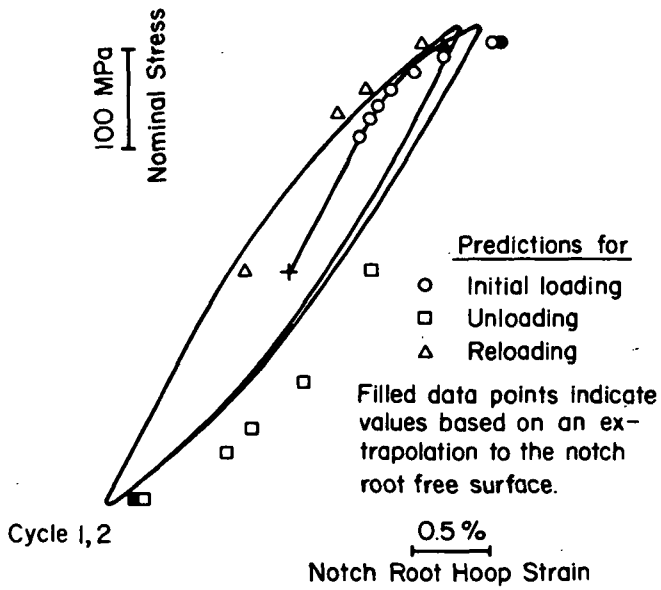

(a) During the first three load (stress) reversals.

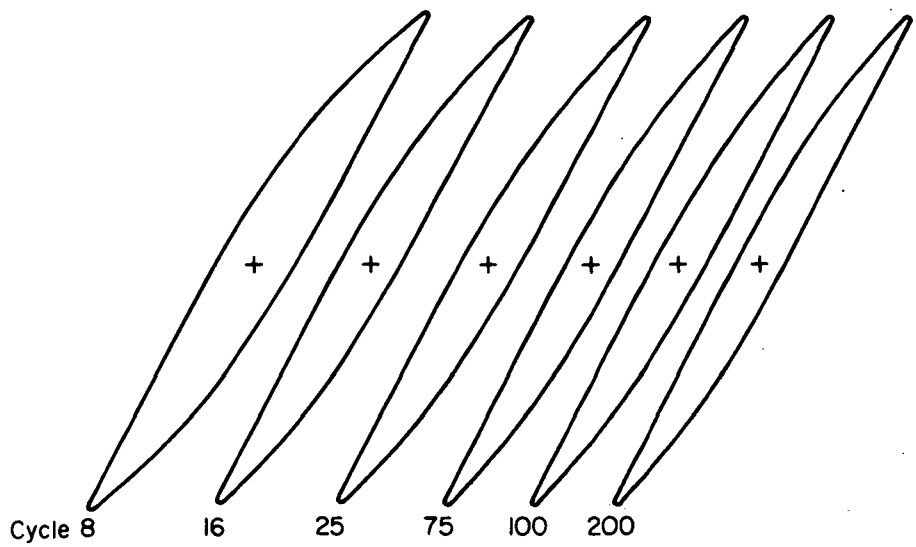

(b) Up to and during stable local response.

Figure 14. – Comparison of observed and analytically determined nominal stress-local strain response under cyclic loading.

response as a function of nominal stress during the first three reversals, for the integration point nearest the notch root (0.0179 cm below the free surface and 0.049 cm away from the transverse net section). Also shown on this figure are experimental hysteresis data for the first three reversals along with that for cycles 8, 16, 25, 75, 100, and 200, for a closely corresponding experimental case. The experimental results shown are for the case where $P/P_y = 1.6$. This case has been shown for comparison with the analytical case of $P/P_y = 1.5$ to emphasize the experimentally observed difference in strain due to cyclic hardening, this difference being proportional to the magnitude of local strain. Note that the experimental results for the first few reversals show that the nominal stress-local strain response cannot be exactly represented as an odd mathematical function because the branches are not congruent. Thus, not surprisingly, transient response and the attendant stress-strain redistribution preclude exact simulation via the total (deformation) theory of plasticity, at least during the period of significant transient response. However, as the transient effect diminishes, the experimentally developed hysteresis branches become increasingly congruent so that the cyclic nominal stress-strain local response could, indeed, be modeled by an odd function used in conjunction with appropriate memory rules in accordance with the deformation theory, as detailed in Reference 38. In view of these observations and the significant transient inelastic action involved in the analytical simulation of the nominal stress-local strain response via the FEM, the predicted response over the first three reversals should not be congruent if the finite-element method suitably models the physical reality. Examination of the predicted response clearly indicates this lack of congruence, thereby providing support for the validity of the analytical results presented in Figure 13(a). This, coupled with the close correspondence between the predicted and observed response shown respectively in Figures 13(b) and 8(c), suggests that the transformation from nominal stress to local strain for subsequent use in fatigue damage computations has been suitably established by the FEM, at least for the notched specimen geometry of interest in this program.

FATIGUE ANALYSIS

The Approach – Assumptions, Limitations and Discussion

In using the smooth specimen fatigue data discussed in the previous section to assess fatigue damage at a notch root, a simple two-step approach is employed. As noted earlier, the first step is to accurately determine strains and stresses at the notch root in terms of applied loads or nominal stresses. This has been accomplished in the present program via the FEM, as just outlined. The second step is to assess fatigue damage using these strains and stresses and smooth specimen fatigue data. Factors governing the fatigue process (the rate of damage accumulation) are assumed to be matched in the smooth specimen and at the notch root by using smooth specimen data with a value of some appropriate damage parameter equal to that at the notch root. These steps are repeated and damage summed for each load reversal (in sequence) until failure is indicated in accordance with some failure criterion. This two-step approach has its roots in the early work of Smith[39] in 1962. Later, Grover[40] recognized the importance of careful "attention to local stresses and strains" in life prediction. More recently, Crews and Hardrath[41] and Topper and his coworkers[42-44] have made life predictions of singly notched coupons via this approach. (Note, the terminology "singly notched" is taken here to mean laboratory test specimens which contain symmetrically placed geometric stress raisers of a single value of stress concentration, e.g., central hole, edge fillets, edge radii, etc.)

Underlying the current use of this approach which employs a deformation-type plasticity analysis are two basic assumptions. Firstly, it is assumed that deformation theory is valid for plastic strains. The second assumption is that equal deformations at critical locations as measured by the energy-based damage parameter[22] lead to equal numbers of cycles to the completion of crack initiation at all such locations. This correspondence is, of course, limited by the scatter caused by the random nature of the fatigue process. Conditions required for these assumptions to be valid are discussed later in this section. However, it should be noted at the outset that the conditions imposed herein for ensuring the validity of the second assumption restrict

calculations to predicting a crack-initiation period short enough that similitude in the cracking process is maintained between reference smooth specimens and the notch roots for which predictions are to be made.

Previous applications of this two-step approach have often failed to properly define failure and to match conditions at the failure locations in smooth specimens and at notch roots. Because failure was almost always defined by specimen separation and not crack initiation in previous applications, the cracking processes were often dissimilar. Also, uniaxial smooth specimen data were often used in applications where the notch root stress state was not uniaxial. Under such conditions, the equal deformation - equal life assumption was invalid. Additionally, in many previous applications of the approach, the use of inaccurate and sometimes inappropriate "universal notch analyses" to transform nominal stress into critical location strains and stresses led to inaccurate calculations of notch root stresses and strains. Each of: separation used as a failure criterion; using smooth specimen data taken in tests of smooth specimens with crack-initiation conditions not matching notch root conditions; and using inappropriate stress analyses has significantly contributed to the confusion encountered in previous efforts to relate smooth and notched specimen fatigue life data.[6-8, 24, 28] However, when conditions for similitude in the failure processes in smooth and notched specimens were ensured, accurate life predictions have been made.[24, 28, 45] This section examines conditions for similitude in the context of notched fatigue specimens. Then, suitable analytical expressions of the transformation of nominal stress to local stresses and strains are introduced and their use in fatigue analysis outlined. Finally, the assumptions and limitations are enumerated and discussed.

Similitude in the Fatigue-Damage Processes in Smooth and Notched Specimens

As noted in the previous section, life predictions for notched specimens will be based on fatigue data obtained from smooth specimens. In this procedure, it is assumed that the notched specimen for which the fatigue life is being predicted will form a fatigue crack at the same life as a smooth specimen if there is similitude in the crack initiation processes in the two samples.

This assumption by itself is undoubtedly valid. Identical local conditions at the crack initiation sites of notched and smooth samples throughout the crack-initiation period would result in identical crack initiation lives. What is more difficult to ascertain is the degree to which the assumption of similitude and the corresponding equality of fatigue lives of smooth and notched samples is sensitive to small differences in each of the variables affecting the fatigue-damage process.

It will be assumed for the present that when factors such as temperature and chemical environment are held constant, the crack-initiation processes will be identical in smooth and notched specimens so long as the strain fields around the tips of the initiating cracks are virtually identical for a distance equal to several times the current length of the crack. Consider the case of a crack tip in a notched specimen. It is clear that as the radius of the notch decreases, the region over which strains at the notch root approximate to a given level of accuracy those in a smooth specimen also decreases. Therefore, to match strains in notched and smooth specimens to a given level of accuracy, the maximum allowable crack length will decrease with decreasing notch radius. Given a quantitative correlation between the nondimensional ratio of notch root radius to crack length and the accuracy with which strains at the crack in a notched specimen reproduce those at a crack of equal length in a smooth specimen, the limit of this ratio to give any desired degree of accuracy could be determined. Clearly, there is a lower limit beyond which this rationale is invalid, in that, as the root radius approaches a size on the order of the metallurgical features of the material, the lower limit of range of applicability of continuum mechanics is reached. A second similar consideration in this context relates to the minimum volume of material at critical locations necessary for the locations to be considered metallurgically homogeneous (identical). While this latter consideration may be important for very small notch root radii, recent work indicates the contribution of this aspect to a possible size effect is negligible, at least for notch radii of engineering interest.[27]

Because solutions such as those noted above are not generally available in an analytical form, it is necessary to determine a desirable ratio indirectly from available fatigue data. For practical reasons, a small

limiting crack length is arbitrarily chosen as constituting the end of crack initiation. The minimum notch radius for which notched specimens having the same local strains as smooth specimens then delineates the minimum radius for which fatigue predictions can be made.

A number of factors influenced the somewhat arbitrary crack length of 0.01 cm which has been used herein to define the end of crack initiation. Firstly, it was thought to be conveniently measured in the laboratory but was still small compared to the radius of most notch radii of practical interest. Furthermore, notches sharp enough to have radii approaching this length have very short crack-initiation periods and spend virtually all their life in crack propagation. For such cases, other approaches such as Fracture Mechanics are superior to the present approach. A crack length of 0.01 cm is also on the order of the length attained by the nonpropagating cracks found in sharply notched specimens at low stress levels but not in smooth specimens. Consequently, this definition of crack initiation will admit these cracks, the formation of which is correctly predicted by the present approach.[28]

It should be noted that in considering similitude, it has been assumed that smooth specimen data representative of the environment, stress state, and mean stress at a notch root are available to allow a direct matching of stresses and strains in notched and smooth specimens. Since this is not usually the case, the fatigue data for the appropriate environment for a smooth specimen of interest will be approximated using the energy-based damage parameter[22], shown earlier in Figure 10(b) to suitably consolidate mean stress effects.

Assumptions and Limitations

In situations where similitude in the fatigue processes in smooth and notched specimens exists, available fatigue data indicate that the equal damage - equal life assumption is valid. An extensive statistical examination of these data showed that the assumption was indeed realistic[28], provided that damage is assessed using a damage parameter comparable to the energy-based form. Likewise, the comparison of smooth and notched specimen crack initiation fatigue resistances of the present study indicates the validity of this assumption (cf, Figures 11(a) and 11(b)). Thus, as in References

27 and 28, one can further conclude that "size effects" concepts[46-51] are superfluous in making life predictions of notched specimens using smooth specimen data. As a consequence, damage can be assessed directly in terms of local stresses and strains determined by the first step in the two-step life prediction procedure. In fatigue applications, transient response complicates the determination of local strains from the nominal stress - local strain transformation, as noted in the previous section and as evident in the noncongruent hysteresis paths shown in Figure 14. But when a stable cyclic state is approached early in life, the error in computing local strain through the reversal-by-reversal application of the deformation theory of plasticity in fatigue analysis[38] is small. Because a stable cyclic state is asymtotically approached early in life, fatigue analysis would be most accurate if the stable transforation is employed.

In addition to the requirement that the deformation response be cycle invariant, there are other necessary conditions to ensure the validity of the first transformation. These conditions are apparent from a consideration of the general mathematical form of the transformation,

$$\Delta\underset{\sim}{\varepsilon}^{t} = f(\Delta\underset{\sim}{S}) \quad , \tag{1}$$

where $\Delta\underset{\sim}{\varepsilon}^{t}$ represents the local total strain state and $\Delta\underset{\sim}{S}$ represents the external stress state. This unique relationship (one-to-one correspondence) between nominal stress and local strain implies path (history) independence in addition to cycle invariance. Furthermore, this unique relationship implies that all elements of material throughout the body (notched component) deform in phase with the external load, a situation which exists only if the external loads are in direct proportion to each other (proportional loading). Thus, equations of the form of Equation (1) are valid only when used to relate nominal stress to local strain in a proportionally loaded component (local and global bifurcation assumed precluded) fabricated from a material whose stress response is cycle invariant (stable).

The above-noted 3 conditions (1) proportionally stressed critical location, (2) proportionally loaded component, and (3) cycle invariant (stable) material stress response are seldom satisfied simultaneously in practical

applications. Fortunately, for the present case -- that of a thin, notched plate -- all are satisfied once the asymtotic state of stability is approached. The reversal-by-reversal application of the results of the finite-element stress analysis in accordance with the deformation theory is thus considered valid in the present application.

Convenient Analytical Characterizations of the Transformation

There are two convenient forms of the nominal stress to local strain transformation useful in determining local stress and strain for use in notch root damage computation as a function of nominal stress.

One convenient form of this transformation makes use of the Neuber parameter.[5,6] This parameter was previously developed to facilitate calibration of Neuber's rule[52] as applied in fatigue analysis for application to a specific notched specimen geometry and material using the results of stress analyses or measured local deformations, as detailed in References 49 to 51. To evaluate this Neuber parameter, local stresses and strains determined from these accurate stress analyses or measurements are used to compute a "theoretical fatigue notch factor" defined by

$$K_f^t = \frac{(\Delta\bar{\sigma} \cdot \Delta\bar{\epsilon}^t \cdot E^*)^{1/2}}{(\Delta\bar{S} \cdot \Delta\bar{e}_n^t \cdot E^*)^{1/2}} , \qquad (2)$$

where E^* is the modulus given by $E^* = 3E/2(1 + \nu)$, $\Delta\bar{\sigma}$ and $\Delta\bar{\epsilon}^t$ are ranges of equivalent notch root stress and total strain, and $\Delta\bar{S}$ and $\Delta\bar{e}_n^t$ are ranges of equivalent nominal stress and total strain. The Neuber parameter, defined by the ratio of K_f^t to K_t, is thus a measure of the difference between values of local strains and stresses found from accurate stress analyses and those found by the use of Neuber's rule as a universal notch analysis. In applications such as the present where the scope is limited to nominal elastic response, the Neuber parameter has the form

$$P = \frac{K_f^t}{K_t} = \frac{(\Delta\bar{\sigma} \cdot \Delta\bar{\epsilon}^t \cdot E^*)^{1/2}}{K_t \, \Delta\bar{S}} \quad . \tag{3}$$

A second form of this transformation that also can be conveniently employed in fatigue analysis has its basis in the observation that the relationship between nominal stress and inelastic notch root strain in singly notched specimens follows a power-law equation[38]. Thus,

$$\Delta\bar{\epsilon}^t = \Delta\bar{\epsilon}^e + \Delta\bar{\epsilon}^P = K_f^t \frac{\Delta\bar{S}}{E^*} + \left(\frac{\Delta\bar{S}}{K_2}\right)^{1/n_2} \tag{4}$$

$$K_f^t = \frac{\Delta\bar{\epsilon}E^*}{\Delta\bar{S}} - \frac{E^*}{\Delta\bar{S}}\left(\frac{\Delta\bar{S}}{K_2}\right)^{1/n_2} \quad . \tag{5}$$

The parameters K_2 and n_2 are chosen so as to numerically best fit Equation (5) to the relationship between nominal stress and notch root strain found from stress analysis (or notch root strain measurements) for the notched component geometry and material of interest. When the values of K_2 and n_2 are determined from "stable" notch root behavior they are denoted K_2' and n_2'.

Note that when the deformation response at the notch root is elastic and the local stress state is uniaxial, Equations (2) and (4) reduce to

$$K_f^t = \frac{\Delta\sigma_1}{\Delta S} \quad .$$

The value of K_f^t computed using either Equation (2) or (4) is the predicted value of the observed fatigue concentration factor. Equations of the form of (2) and (4) have been shown to provide accurate crack initiation life predictions for a variety of notched specimen geometries made from many engineering materials (e.g., References 6, 8, 27, and 45). Their successful application has been shown to require similitude in the fatigue process at fatigue critical locations of notched specimens and the smooth specimens used to determine reference fatigue data. It has also been shown to require that notch root deformations be both accurately determined from stress analyses (or measured strains) and adequately represented in the smooth specimen simulation of notch

stress-strain behavior. All such successful applications of this approach have made use of a smooth specimen damage-life relationship such as that shown in Figure 10(b) to transform the local strains (and corresponding stresses) into fatigue damage. They have utilized a linear damage accumulation law and when applied to constant amplitude loading such as in this research have defined damage per reversal as the inverse of the life to crack initiation associated with the computed value of the damage parameter (the ordinate on Figure 10(b)). In the present constant amplitude case, there is no need to account for sequence effects by the application of some nonlinear damage accumulation law[54]. Neither is it necessary to apply sophisticated cycle counting rules to resolve the notch root stress-strain response into cycles and connecting hysteresis segments as in variable amplitude damage analysis (i.e., memory rules do not have to be invoked[38]). Transformation of the local stress-strain response into damage is thus a straightforward process.

Local stresses for use in this damage assessment are assumed to be related to local strains through the uniaxial stress-strain equation of the material (a valid assumption for the "thin" notched plates used in this study[45]). In particular, the maximum local stress required in damage computations has been assumed equal to that attained at the first strain reversal, an assumption consistent with observed material mean stress response under strain control (cf, earlier discussion of response in the section Derived Data).

Mathematical Model for Life Prediction-Adaptation to Data Consolidation

The Life Prediction Model

Based on the foregoing discussion, the essential features of the mathematical model for life prediction developed under this contract are similar to those of the previous consolidation studies carried out by BCL under contract to NASA Langley Research Center[1-3]. Clearly, both the past and present programs make use of a two-step (transformation) life prediction process; although the transformations may not have been delineated in the previous work, they were nevertheless the same. A second similarity is the manner of damage accumulation in accordance with a linear damage rule. There are, however, major differences in the means of damage assessment.

With regard to damage assessment, the present study utilized an energy-based damage parameter[22] which, for uniaxial stress states, has the form of the Smith-Watson-Topper parameter[20]. In turn, this parameter is a special form of the Walker parameter[23] utilized in earlier studies, the difference being in the value of the exponent. Examination of the results of References 1 through 3 indicate that the difference in data consolidation achieved by the use of this marginally different form of damage parameter compared to the optimized parameter used previously is not significant. In addition to the use of this slightly different damage parameter, plastic strain has also been employed as a damage parameter. This parameter has been shown to provide a very good basis for damage assessment at very large strains[19]; but, as expected, it fails to consolidate mean stress data at long lives. The damage parameter assumed to govern in life prediction is that associated with the lowest indicated rate of damage accumulation— at long lives, the mean stress parameter controls, while at shorter lives, the plastic strain parameter controls.

In the context of determining the local strains and stresses from nominal stress, significant differences exist between the present and previous programs. There are two primary differences. First, the present program utilized accurate stress analysis to establish this transformation whereas the previous studies made use of inappropriate "universal notch analysis" that have been shown to be erroneous.[6,7,28] Second, the present program does not resort to the use of a somewhat arbitrary "size effect" whereas the previous studies have. There are other related differences; in particular, the means of determining the maximum stress at the notch root under mean stress conditions. But, computations indicate that for the aluminum alloy of interest these differences are minor.

The important emperical relationships used in the life prediction procedure are the first transformation (Equation (4)) -

$$\frac{\Delta\varepsilon}{2} = \frac{2.58\ \Delta S}{69.59 \times 10^{3}} + \left(\frac{\Delta S}{19.16 \times 10^{-8}}\right)^{3.57} \quad ; \qquad (4(a))$$

and the monotonic stress-strain response -

$$\frac{\Delta e}{} = \frac{\Delta s}{69.59 \times 10^{3}} + \left(\frac{\Delta s}{1355.5}\right)^{13.16} \quad . \qquad (6)$$

For the second transformation, the equation used for plastic strain-life damage assessment is

$$\frac{1}{D_R} = 2N_i = 0.19 \left(\frac{\Delta e^p}{2}\right)^{-1.29} \quad ; \qquad (7)$$

while that for the damage parameter is

$$\frac{1}{D_R} = 2N_i = K_e \left(\frac{s_{mx}\, \Delta e^t/2}{6.89}\right)^{m_e} \qquad (8)$$

where K_e and m_e have values of 381, -1.91 and 1.8×10^{-4}, 9.07 for values of S/6.89 bounded respectively as follows: $22 < S/6.89 < 4.3 \times 10^{-2}$ and $4.3 \times 10^{-1} < S/6.89 < 6 \times 10^{-2}$ and, D_R and $2N_i$ designate the damage per reversal and the number of reversals to initiation, respectively. Both Equations (7) and (8) had cutoffs beyond which the damager per reversal has been considered negligible. In both cases, this cutoff has arbitrarily been selected as 2×10^7 reversals, a value chosen based on a consideration of the smooth specimen damage-life behavior at long life. The factor 6.89 is a units correction.

The life prediction process based on these mathematical models is straightforward. First, the peak notch root strain is determined from the corresponding peak nominal stress using Equation (4(a)). The corresponding maximum notch root stress is next determined from Equation (6). The third step is to compute the minimum notch root strain and thereafter compute the local strain range. Using the maximum stress and this total strain range, the plastic strain amplitude is next computed. The fourth step is to compute damage per reversal (life) using each of Equations (7) and (8).

Adaptation for Fatigue Life Data Consolidation

Any fatigue-life prediction model can be conveniently adapted for use in data consolidation, once a basis for consolidation is established. With regard to the possible variables which could be used as a basis, there are two. First, computed damage at a given life to crack initiation could be used. Alternately, predicted life at a given nominal stress level could be employed. Previous BCL studies conducted under contract to NASA Langley Research Center[1-3] have made

use of the first of these. As such, the influence of the failure criterion on the extent of consolidation could not be directly assessed. Note, too, that this basis is somewhat insensitive compared to life-based measures at long lives, an advantage in some respects (for example in culling run-out data).

Because of the impact of the choice of the failure criterion on the accuracy of life predictions[28] and the desire of the present program to assess this aspect and retain sensitivity at long lives, the ability of the improved method of life prediction to affect data consolidation will be assessed hereafter in terms of the ratio of predicted to observed fatigue life. Values of this ratio will be examined as a function of the observed life. Throughout, predicted life will be that computed using smooth specimen data as outlined in the preceding paragraphs. As such, smooth specimen data reported in Table 2 ($K_t = 1.0$) are consolidated to the extent that the empirical damage rate equation used in the notch root damage assessment best fit those data. This consolidation is, therefore, achieved to the greatest extent possible - the ratio of predicted to observed life being 1.01 with an estimated value of the population standard deviation of 0.4106. (The distribution is skewed towards values of the ratio less than one. If the extremes of the distribution are censored, the distribution is essentially normal with a mean of 0.91 and an estimate of the population standard deviation of 0.1756.) Subsequent examination of the data consolidation of notched specimens is, therefore, superimposed on a very effective smooth specimen data consolidation.

It is noteworthy that in the previous studies[1-3], differences in the mean fatigue resistances for cases where $K_t = 1.0$ and $K_t > 1$ are substantial. Thus, these previous studies consolidated notched specimen data independent of the smooth specimen results. Smooth specimen data assembled under these previous programs and that reported in the literature (data from References 5, 9, and 11) are consolidated to varying degrees in the context of the smooth specimen mean life response for the data developed in this program. For the strain-controlled data developed recently as reported in Reference 5, the mean value of the ratio is 0.959 with a standard deviation of 0.564. These data and that of the present program Table 2) are, therefore, in close correspondence. With regard to the data reported in References 9 and 11 developed in the early 1950's using load-controlled testing in subresonant systems, the mean value of the

ratio is 1.793 with a standard deviation of 3.1. The mean value of the life ratio indicates that these data had a slightly greater fatigue resistance than that indicated by modern strain-controlled testing.

The level of consolidation of the above-noted data is not high as indicated by the large value of the standard deviation. Such an increase in scatter can be due to the differences in test technique (1) between the various laboratories used to develop these data (cf, Reference 11, Figure 21) and (2) between the era of the early 1950's and today. Unfortunately, the influence of test technique on the mean value of and the scatter in the life ratio cannot be established. But, fortunately, this does not create a serious problem in later assessing the extent of notched specimen consolidation. This is so because the mean resistances do not differ substantially (all data developed via strain-controlled testing lie well within the $\pm$ 1σ scatter band of the load-controlled data reported in References 9 and 11). In this same context, it is noteworthy that the mean resistance of these strain-controlled data provides the best mean curve for the totality of the data developed in the early 1950's (compare the present data with that of Figure 28 of Reference 11). Thus, it is valid to assume that these strain-controlled data provide a valid basis to assess the rate of damage accumulation at notch roots in the corresponding notched specimens, data for which are reported in References 12 and 55. This assumption is invoked later in the section dealing with notched specimen data consolidation.

CONSOLIDATION OF 24-SERIES ALUMINUM ALLOY NOTCHED SPECIMEN FATIGUE LIFE DATA – DISCUSSION

The improved method of fatigue life prediction has been applied in the context of data consolidation as detailed in the previous section to a variety of data, the purpose being to assess the improvement in consolidation as compared to that achieved in the previous studies. Several data sets have been examined; the common feature being the generic material, the 24-series aluminum alloy. Within this overall data set are several subsets which, for the most part, represent data assembled under the previous program. These data, reported in References 5, 12 and 55, are supplemented by the notched specimen data developed in this program. Specific data subsets considered

are: (1) new data from this program for open hole sheet specimens; (2) data for open hole sheet specimens from Reference 5 pooled with (1); (3) data for open hole sheet specimens from Reference 12; (4) data for open hole sheet specimens from Reference 55; and (5) all data for open hole sheet specimens pooled into a single data set. Data consolidation for each of these subsets is considered in turn in the ensuing paragraphs.

Consider first the consolidation achieved for the results presented in Table 3. The mean value of the ratio of predicted to observed lives (hereafter designated as "ratio" for this case when separation has been used as a failure criterion was 0.472 with a standard deviation of 0.327. In every case, the Smith-Watson-Topper parameter (hereafter designated as SWT) controlled life. When the failure criterion was changed to one of initiation by subtracting the propagation period (based on the response shown in Figure 8(d)) from the total life to define the observed life, the mean value of the ratio became 0.567 with a standard deviation of 0.337. This mean value of the ratio is somewhat less than unity indicating that, on the average, the improved crack initiation life prediction model is slightly conservative. In terms of the ability of the model used in the previous studies to simultaneously consolidate smooth and notched specimen data, the present model is apparently improved. This is evident by comparing the respective mean life curves (Figures 7 and 8 of Reference 2) which differ on the average by more than a factor of $\pm$ 8 on life (i.e., the mean value of the life ratio is greater than $\pm$ 8). With regard to the degree of consolidation achieved, comparison of the respective values of standard deviation shows the dispersion of these notched data to be somewhat less than that of the corresponding smooth data. Thus, these data are highly consolidated. It should be emphasized that the present comparison of the current model to the previous one is not direct. That is, the data sets considered differ in content and size. Such comparisons will, however, continue until in the final comparison the data sets will match identically.

Consider next the consolidation of the above notched specimen data pooled with similar data reported in Reference 5. This pooled data set represents 33 specimens. Consolidation of these data using the improved crack initiation life prediction model is comparable to that achieved as detailed above. The pooled mean value of the life ratio for these data when separation was used as a failure criterion is 0.472, with a standard deviation of 0.334. When

initiation is used as a failure criterion, the corresponding mean is 0.612, with a standard deviation of 0.415. Clearly, the choice of the failure criterion significantly influences (increases) the accuracy of the life prediction; it also appears to slightly increase the data dispersion. In general, the consolidation of these data is uniform over the range of lives reported, as evident in Figure 15. As with the consolidation of data developed as a part of this investigation, this pooled data set shows the life prediction model to be slightly conservative. Likewise, this pooled data set shows the present life prediction model to be apparently improved as compared to that of the previous studies[1-3]. Again, as with the data developed during this investigation, the dispersion of the notched specimen data is slightly less than that for the smooth specimens. Thus, the improved life prediction model affects a high degree of data consolidation for both smooth and notched specimens.

Consider next the results of the open hole sheet specimens reported in References 12 and 55. Clearly, if consolidation of these data is to be achieved, the nominal stress to notch root strain transformation in the life prediction model must be accurate for the notched sheet specimens used in those studies.

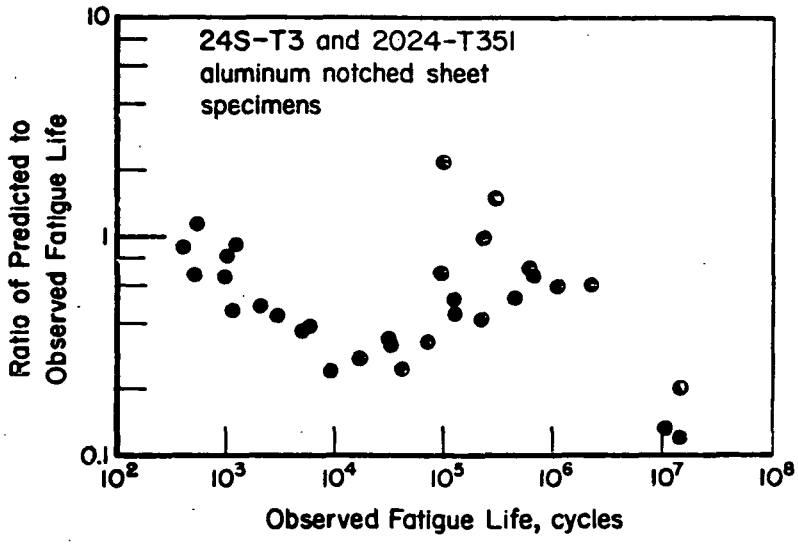

Figure 15. — Data consolidation for 24S-T3 and 2024-T351 notched sheet specimens — data from this investigation and Reference 5.

Fortunately, use can be made of the fact that for a particular type of specimen geometry fabricated from a given material, the transformation for a given geometry is apparently generic to the class[24]. This is evident in Figure 16, reproduced from Reference 24. This figure indicates that a single nominal stress-stable notch root strain transformation characterizes the response measured in open hole notched 24-series aluminum alloy sheet specimens for five specific geometries,[4,5] including that of this investigation. This same transformation can, therefore, be assumed accurate for the open hole specimens, results for which have been reported in References 12 and 55.

It should be noted that data shown in Figure 16 have been obtained from "thin" notched specimens for which the local stress state is essentially uniaxial. Such a state also prevails at the notch root for the data reported in Reference 12, while that of Reference 55 exhibits various degrees of local biaxiality. The role of biaxiality in altering this transformation has been accounted for in the transformation as detailed in Reference 45; as such only the elastic component of the local strain has been adjusted. Unfortunately, the role of biaxiality under the action of inelastic strains has not yet been analytically determined. Accordingly, no adjustment of the plastic component of the notch root strain has been made.

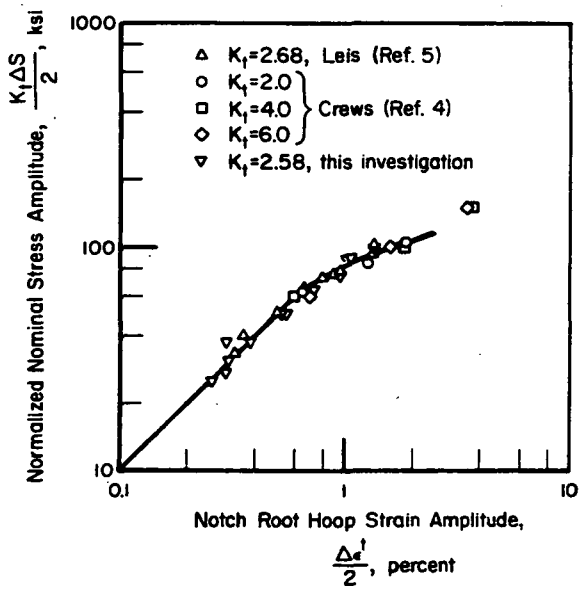

Figure 16. — Normalized nominal stress-local strain response for notched 24S-T3 and 2024-T351 aluminum alloy sheet specimens.

It is also important to note that the data sets in both References 12 and 55 contain several run-outs. Additionally, there are numerous data developed for lives much in excess of 2×10^7 reversals, the life beyond which the damage accumulation rate becomes negligible and analysis predicts a run-out. Neither case should be included in the assessment of the ability of the improved crack initiation prediction model. This is especially true of actual run-outs since cracks did not initiate. Consequently, actual run-out data have been censored. Predicted run-out data have, however, initially been included. In both of the ensuing assessments, only cases for which a crack initiation criterion has been used will be examined in detail.

Results of the consolidation of the open hole notched sheet specimen data of Reference 12 gave rise to a mean value of the ratio of 0.317 with a standard deviation of 0.227. These results were based on an initiation failure criterion empirically derived from the results shown in Figure 8(d). Of these the plastic strain damage parameter governed 5 predictions while the SWT parameter governed 24. There were a total of five results censored on the basis that the maximum net section stress exceeded the yield stress of the material. Only one predicted run-out has been included in this consolidation, a total of five results being censored on the basis that the test result was a run-out. When a failure criterion of separation was used, the values of the mean and standard deviation were 0.306 and 0.218, respectively. These correspond closely with those of the initiation-based consolidation noted above.

With reference to the initiation-based data consolidation, the improved crack initiation life prediction model again is slightly conservative (by a factor of 3.15). This represents an apparent improvement in the accuracy of this life prediction model as compared to that of the previous studies which is nonconservative at short lives and conservative at long lives by more than a factor of $\pm$ 8 in life. In this context, the net improvement in absolute accuracy is better than a factor of 2. Similarly, this improved life prediction model has better consolidated these notched specimen data, the dispersion being more than a factor of 10 less than that for the corresponding smooth specimen data, based on standard deviation. Much of these data fall within the -1σ scatter band of the corresponding smooth specimen data as evident in Figure 17(a). This is in strong contrast to the results of

the previous study which showed distinct data bands for smooth and notched specimens and levels of dispersion greater for the notched specimens as compared to that of the smooth specimens (cf, Table 6 and Figures 7 and 8 of Reference 2).

Consider next the consolidation of the results of Reference 55. This consolidation, based on a total of 457 test results, showed the mean value of the life ratio to be 0.244 with a standard deviation of 0.356 based on a crack initiation failure criterion. Of these test results, the plastic strain damage parameter governed 12 predictions while the SWT parameter governed 445. There were a total of 9 results censored on the basis of gross yield while 23 results were censored based on the run-out criterion. There were a total of 26 predicted run-outs, all of which were based on the SWT criterion. When a separation criterion was used, the respective values of the mean and standard deviation were 0.213 and 0.278. Again these values correspond closely with those based on an empirical initiation criterion.

With reference to the initiation-based data consolidation, the improved life prediction model again is somewhat conservative (by a factor of 5). Nevertheless, this consistently conservative model constitutes a substantial improvement over that of the previous program which is nonconservative at short lives by a factor of 10 and conservative at long lives by more than a factor of 8. The net improvement is, therefore, substantial. Similarly, this model gives rise to a much improved data consolidation. Again, the majority of the data for the notched specimens lie within the $\pm 1\sigma$ scatter band of the corresponding smooth specimen data as evident in Figure 17(b), a result which as noted previously is in strong contrast to the consolidation achieved in the previous study.

Finally, consider the consolidation of the entire data set, results for which are shown in Figure 17(c) for the case of the initiation-based consolidation of 517 valid (uncensored) test results. The computed mean value of the life ratio is 0.272 with a standard deviation of 0.365. This consolidation essentially mirrors each of those discussed previously. The mean value is somewhat dominated by the data of Reference 55, although it is within a factor of about 2 of the mean for any one data set. The standard deviation is likewise dominated by the largest data set, but it too is representative of all data sets, the extremes being 0.277 and 0.415. This consistency among the

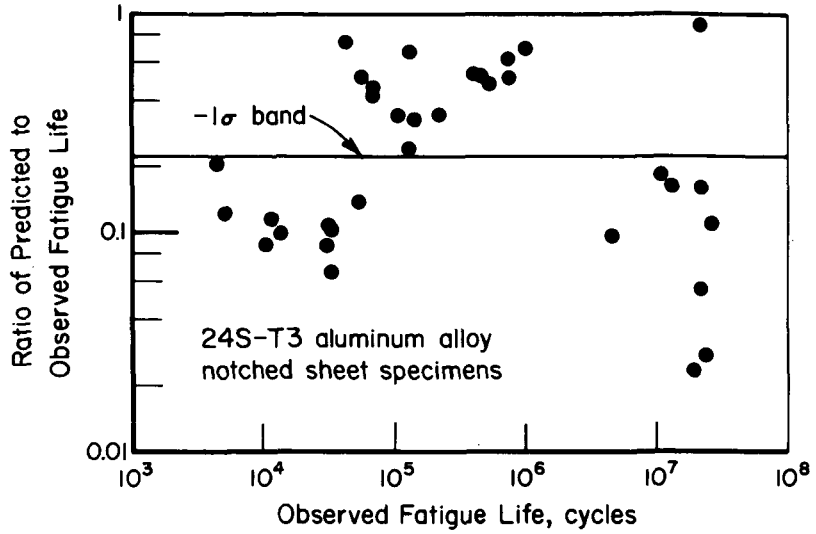

(a) Data from Reference 12.

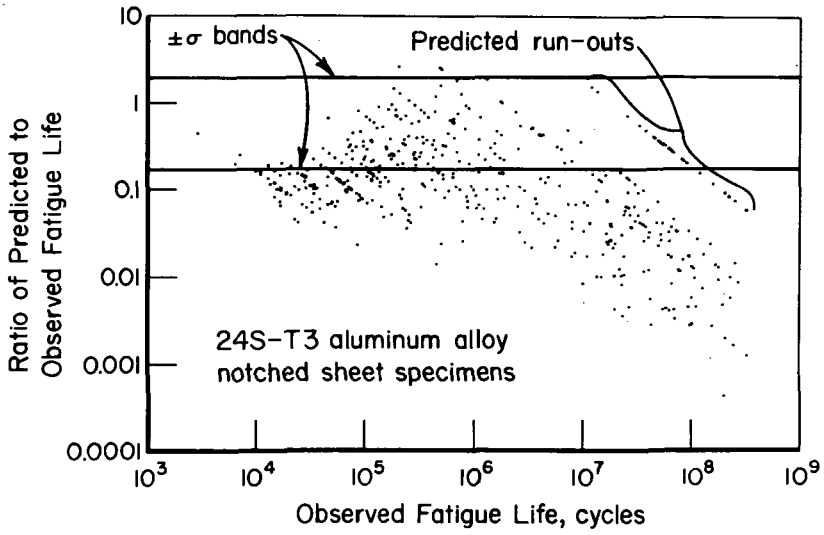

(b) Data from Reference 55.

Figure 17. — Data consolidation for 24S-T3 and 2024-T351 notched sheet specimens.

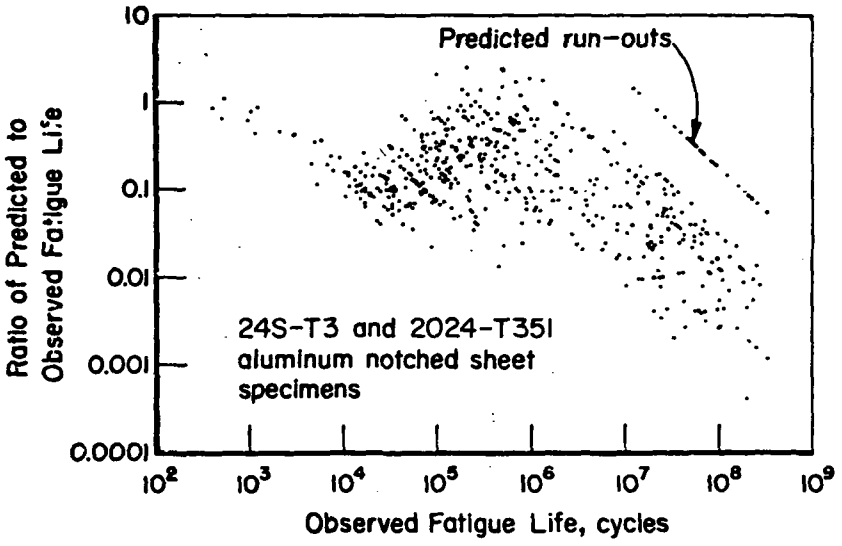

(c) Data from this investigation and References 5, 12, and 55.

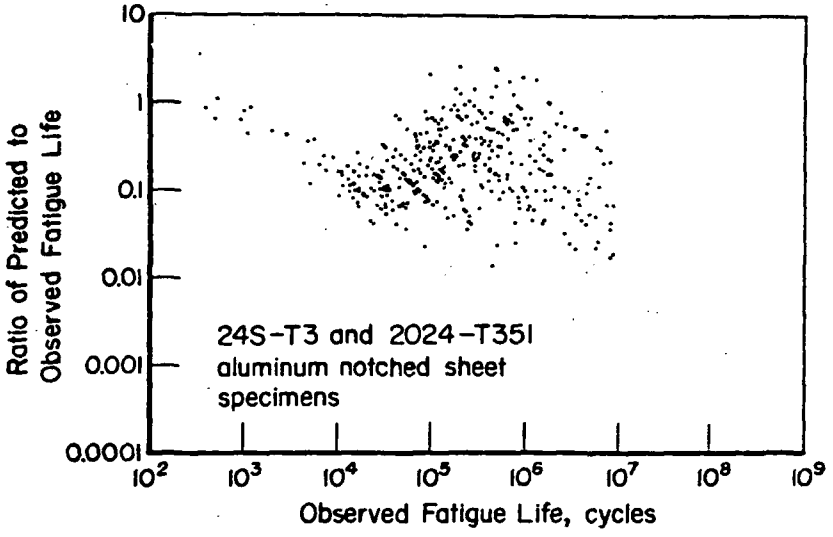

(d) Data from this investigation and References 5, 12, and 55 culled to exclude lives beyond 10^7 cycles.

Figure 17. – (Concluded).

results for the various data sets is significant; it indicates that the life prediction model treats all results in a similar fashion and does not introduce bias or cause banding in the results of the consolidation. This is in contrast to the results of the previous program which tended to show banding in the long life data (particularly that of Reference 55). Another factor of importance is the tendency in the consolidation to fall off at longer lives as evident particularly in Figures 17(b) and 17(c). This is due in part to the failure of the two-segment SWT damage equation to adequately model the rapidly changing damage-life relationship in the very long life regime. It is also due in part to the arbitrary value of the cutoff life beyond which damage per cycle is considered negligible. This is so because all predictions must lie below a line with slope of -0.5 which passes through the coordinate point of unity and the cutoff life. Such a line plots the predicted run-outs and forms an upper bound to the value of the life ratio. Beyond this cutoff life, crack initiation life predictions are by definition invalid since the cutoff implies cracks never initiate. Accordingly predictions beyond this line should be culled from the data set. This results in a net improvement in the accuracy of the life prediction and serves to decrease the overall scatter in the life ratio as evident in Figure 17(d). Further discussion of this pooled data set would repeat previous comments regarding the degree of consolidation in that these data follow the consistent pattern evident in the four previous consolidations. Note that for this data set, which matched identically that of Reference 2, there is a significant improvement in consolidation.

COMMENTARY

For the most part, the individual aspects of this research program were successfully married and culminated in a method of crack initiation life prediction which substantially improved data consolidation, as compared to the results of the previous program. Particularly, this improved model was more accurate in an absolute sense and gave rise to a collapse of notched specimen data greater than that of the corresponding smooth specimen data. Simultaneous consolidation of both smooth and notched specimen data was achieved.

Unfortunately, the program was not without shortcomings, particularly in the inability of the eddy current device to detect cracks on the order of 0.1 mm. Experimental difficulties in this regard necessitated adopting an initiation crack size somewhat larger, on the order of 0.9 mm. These experimental problems were fortunately overshadowed by the remarkable performance of the notch root strain transducer. This device was a consistently good performer, yielding reliable information that was invaluable in verifying the results of the finite element analysis of the notch root stress-strain distribution.

While, in general, the results of this program demonstrate the viability of accurate crack-initiation life prediction methodology to simultaneously consolidate smooth and notched specimen fatigue-life data, they are not conclusive. There are several reasons for this. First the present program has addressed analysis of data for only the 24-series aluminum alloy. It, therefore, presents a very limited basis for establishing conclusively the viability of accurate life prediction analysis to achieve consolidation. Second, the use of data for materials such as the 24-series aluminum alloy does not constitute a severe test of the accuracy of life prediction models. As clearly evident in Figures 18(a) and (b), steels pose a much more severe test, particularly those which cyclically soften. Third, the present study has focused for the most part on results of "thin" notched specimens with essentially local uniaxial stress states. Yet, the majority of notched data in the literature has been developed using geometries with a local biaxial stress state. (Furthermore, most practical geometries are locally multiaxial.) Since stress state effects on consolidation are significant[45] and in general not yet explored under the action of cyclic plasticity, multiaxial effects remain, in general, a conundrum. Finally, the fourth reason is that the present program has examined only the constant amplitude case. Consolidation under variable amplitude loading is an unknown — there being substantial additional complication of both transformations in dealing with variable amplitude loading.

Future work related to improving the current consolidation technology should address each of the above four limitations. Without the results from such studies, the viability of accurate life prediction models to consolidate fatigue life data cannot be conclusively established. In the context of comparisons between this and the previous studies which showed the improvements

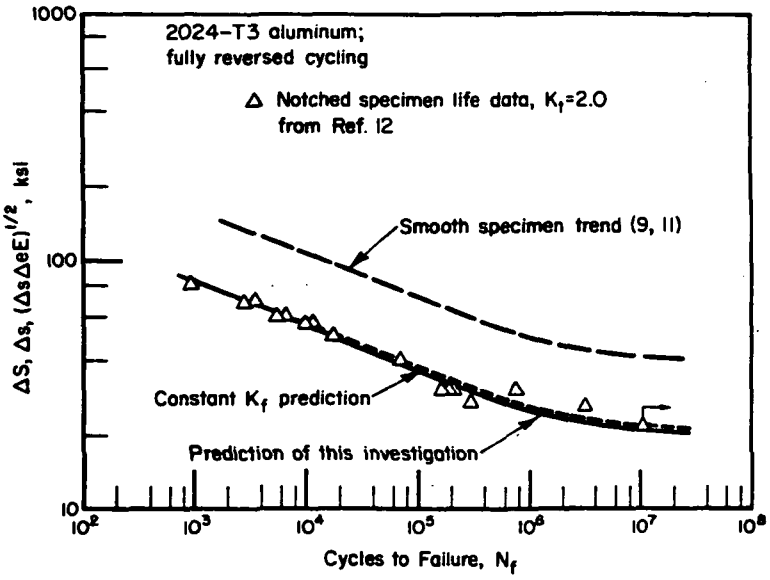

(a) Predictions for 24S-T3 aluminum alloy notched sheet specimens.

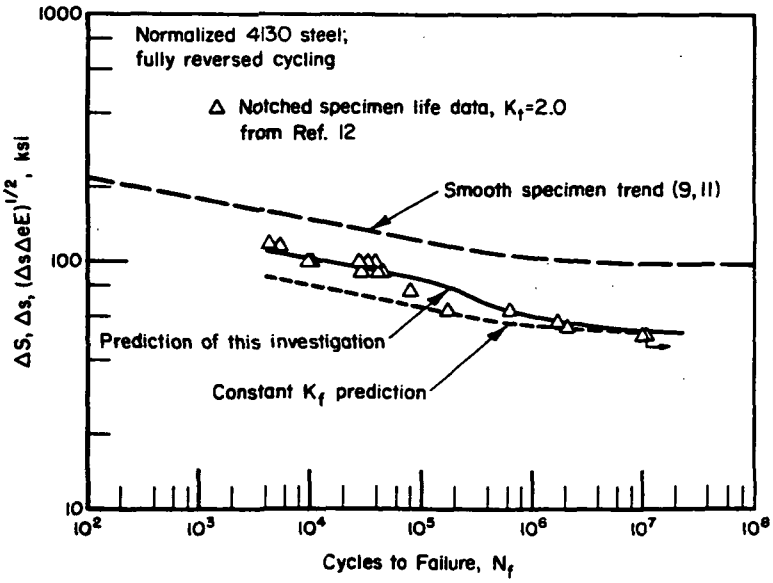

(b) Predictions for SAE 4130 steel notched sheet specimens.

Figure 18. – Comparisons of life predictions using the methods of the present investigation and that of Reference 2.

being related to an understanding of the fundamentals of the notch root deformation response and damage process, future studies should likewise follow a fundamental scientific approach.

CONCLUSIONS

The most significant single conclusion of this program is that improvements in life prediction technology give rise to measurable improvements in data consolidation. There are several other less significant conclusions which pertain to the specific research activities of this program such as: the finite-element method resulted in an accurate analysis of notch root strain response based on comparisons with experimental data; experimental measurements support the hypothesis that equal damage at critical locations gives rise to equal life to crack initiation; smooth and notched specimen data can be simultaneously consolidated; and accurate crack initiation life predictions of notched specimens can be made using smooth specimen data using the improved life prediction model elaborated herein.

REFERENCES

1. Jaske, C. E.; Feddersen, C. E.; Davies, K. B.; and Rice, R. C.: Analysis of Fatigue, Fatigue-Crack-Propagation, and Fracture Data. NASA CR-132332, 1973.

2. Rice, R. C.; Davies, K. B.; Jaske, C. E.; and Feddersen, C. E.: Consolidation of Fatigue and Fatigue-Crack-Propagation Data for Design Use. NASA CR-2586, 1975.

3. Rice, R. C.; and Reynolds, J. L.: Compilation on Fatigue, Fatigue Crack Propagation, and Fracture Data for 2024 and 7075 Aluminum, Ti-6Al-4V Titanium, and 300 M Steel. NASA CR-144982, 1976.

4. Crews, J. H.: Elastoplastic Stress-Strain Behavior at Notch Roots in Sheet Specimens Under Constant-Amplitude Loading. NASA TN D-5253, 1969.

5. Leis, B. N.: Cyclic Inelastic Deformation Behavior of Thin Notched Plates. M. A. Sc. Thesis, Univ. of Waterloo, 1972.

6. Leis, B. N.; Gowda, C. V. B.; and Topper, T. H.: Cyclic Inelastic Deformation and the Fatigue Notch Factor. Cyclic Stress Strain Behavior-Analysis, Experimentation and Failure Prediction. Spec. Tech. Publ. 519, ASTM, 1973, pp. 133-150.

7. Leis, B. N.; Gowda, C. V. B.; and Topper, T. H.: Some Studies of the Influence of Localized and Gross Plasticity on the Monotonic and Cyclic Concentration Factors. J. Testing and Evaluation, vol. 1, no. 4, July 1973, pp. 341-348.

8. Gowda, C. V. B.; Leis, B. N.; and Smith, K. N.: Dependence of Notch Strength Reduction Factor on Plasticity and Duration of Crack Growth. J. Testing and Evaluation, vol. 2, no. 1, January 1974, pp. 57-61.

9. Grover, H. J.; Bishop, S. M.; and Jackson, L. R.: Fatigue Strength of Aircraft Materials Axial-Load Fatigue Tests on Unnotched Sheet Specimens of 24S-T3 and 75S-T6 Aluminum Alloys and of SAE 4130 Steel. NACA TN 2324, 1951.

10. Anon.: Aluminum Standards and Data. The Aluminum Association, 1975.

11. Grover, H. J.; Hyler, W. S.; Kuhn, P.; Landers, C. B.; and Howell, F. M.: Axial Load Fatigue Properties of 24S-T and 75S-T Aluminum Alloys as Determined in Several Laboratories. NACA TN 2928, 1953.

12. Grover, H. J.; Bishop, S. M.; and Jackson, L. R.: Fatigue Strength of Aircraft Materials – Axial Load Fatigue Tests on Notched Sheet Specimens of 24S-T3 and 75S-T6 Aluminum Alloy and SAE 4130 Steel with Stress Concentration Factors of 2.0 and 4.0. NACA TN 2389, 1951, see also NACA TN 2390, 1951, and NACA TN 2639, 1952.

13. Howland, J. C. L.: Stresses in the Neighbourhood of a Circular Hole in a Strip Under Tension. Phil, Trans. Roy. Soc., vol. 229, A, 1930, pp. 49-86.

14. Peterson, R. E.; and Wahl, A. M.: Two and Three-Dimensional Cases of Stress Concentration and Comparison with Fatigue Tests. Trans. ASME, vol. 58, 1936, pp. A15-A22.

15. Griffith, G. E.: Experimental Investigation of the Effect of Plastic Flow in a Tension Panel with a Circular Hole. NACA TN 1705, 1949.

16. Box, W. A.: The Effect of Plastic Strains on Stress Concentration. Proc., Soc. Experimental Stress Analysis, vol. 8, no. 2, 1951, pp. 99.

17. Crews, J. H. Jr.; Hardrath, H. F.: A Study of Cyclic Plastic Stresses at a Notch Root. Exp. Mech., vol. 6, no. 6, June 1966, pp. 313-320.

18. Coker, E. G.; and Filon, L. N. G.: A Treatise on Photoelasticity. Second Ed. Cambridge Univ. Press, 1931.

19. Morrow, J.: Cyclic Plastic Strain Energy and Fatigue of Metals. Internal Friction, Damping, and Cyclic Plasticity. Spec. Tech. Publ. 378, ASTM, 1965, pp. 45-84.

20. Smith, K. N.: On the Design of Metal Structures for Fatigue, with Particular Reference to a Proposed General Stress-Strain Parameter and Notch Factors for Welded Bridges. Ph.D. Thesis, Univ. of Waterloo, 1970.

21. Wetzel, R. M.: A Method of Fatigue Damage Analysis. Ph.D. Thesis, Univ. of Waterloo, 1971.

22. Leis, B. N.: An Energy-Based Fatigue and Creep-Fatigue Damage Parameter. J. Pressure Vessel Tech., Trans. ASME, vol. 99, no. 4, November 1977, pp. 524-533.

23. Walker, K.: The Effect of Stress Ratio During Crack Propagation and Fatigue for 2024-T3 and 7075-T6 Aluminum. Effects of Environment and Complex Load History on Fatigue Life. Spec. Tech. Publ. 462, ASTM, 1970, pp. 1-14.

24. Leis, B. N.: On Deformation and Fatigue Analysis for Cyclically Loaded Notched Components. Ph. D. Thesis, Univ. of Waterloo, 1977.

25. Anon.: Airplane Damage Tolerance Design Requirements. Military Specification, USAF, MIL-A-83444 (tentative), May 1974.

26. Chopra, P. S.: Finite Element Simulation of Secondary Cracking During Brittle Fracture. Ph.D. Thesis, Univ. of Washington, 1971.

27. Leis, B. N.: An Approach for Fatigue Crack Initiation Life Prediction With Applications to Complex Components. Fatigue Life of Structures Under Operational Loads, Proc. 9th Int. Committee Aer. Fatigue Meeting, ICAF Doc. 901, Laboratorium fur Betriebsfestigeit, May 1977, pp. 3.4/1-47.

28. Leis, B. N.; Topper, T. H.: Cyclic Deformation and Fatigue Analyses for Notched Components. Nuclear Eng. and Design, vol. 29, 1974, pp. 370-383.

29. Armen, H.; Pifko, A.; and Levine, H. S.: Finite Element Analysis of Structures in the Plastic Range. NASA CR-1649, 1971.

30. Huang, W. C.: Theoretical Study of Stress Concentrations of Circular Holes and Inclusions in Strain Hardening Materials. Int. J. Solids Structures, vol. 8, no. 2, February 1972, pp. 149-192.

31. Stowell, E. Z.: Stress and Strain Concentration at a Circular Hole in an Infinite Plate. NACA TN 2073, 1950.

32. Budiansky, B.; and Vidensek, R. J.: Analysis of Stresses in the Plastic Range Around a Circular Hole in a Plate Subjected to Uniaxial Tension. NACA TN 3542, 1955.

33. Hill, R.: Plasticity. Oxford Press, 1950.

34. Brown, D. K.: Multivariable Approach to the Finite Difference Solution of Elasto-Plastic Problems. I. J. Numerical Methods in Engr., vol. 10, 1976, pp. 361-377.

35. Zienkiewicz, O. C.: The Finite Element Method in Engineering Science. McGraw Hill, 1971.

36. Bathe, K. J.: ADINA — A Finite Element Program for Automatic Dynamic Incremental Nonlinear Analysis. MIT Rept. No. 82448-1, September 1975.

37. Bathe, K. J.; and Wilson, E. L.: Numerical Methods in Finite Element Analysis. Prentice Hall, 1976.

38. Williams, D. P.; Lind, N. C.; Conle, F. A.; Topper, T. H.; and Leis, B. N.: Structural Cyclic Deformation Response Modeling. Proc. ASCE Spec. Conf. on Engr. Mech., May 1976, in Mech. in Engr., Univ. of Waterloo Press, 1977, pp. 291-311.

39. Smith, C. R.: Small Specimen Data for Predicting Life of Full-Scale Structures. Fatigue Testing of Aircraft Structures. Spec. Tech. Publ. 338, ASTM, 1962, pp. 241-250.

40. Grover, H. J.: Fatigue of Aircraft Structures. Navair 01-1A-13, 1966.

41. Crews, J. H. Jr.; and Hardrath, H. F.: A Study of Cyclic Plastic Stresses at a Notch Root, Experimental Mechanics, Vol 6(6), June, 1966, pp. 313-320.

42. Morrow, JoDean; Wetzel, R. M.; and Topper, T. H.: Laboratory Simulation of Structural Fatigue Behavior. Effects of Environment and Complex Load History on Fatigue Life. Spec. Tech. Publ. 462, ASTM, 1970, pp. 74-91.

43. Topper, T. H.; and Gowda, C.V.B.: Local Stress-Strain Approach to Fatigue Analysis and Design. ASME Paper No. 70-DE-24.

44. Topper, T. H.; and Morrow, JoDean, eds.: Simulation of the Fatigue Behavior of the Notch Root in Spectrum Loaded Notched Members. Univ. of Ill., T & A.M. Rept. No. 333, January, 1970.

45. Leis, B. N.; and Topper, T. H.: Long-Life Notch Strength Reduction in the Presence of Local Biaxial Stress, J. Engr. Mat. and Tech., Trans. ASME, vol. 99, no. 3, July 1977, pp. 215-221.

46. Neuber, H.: Theory of Notch Stresses: Principles of Exact Stress Calculations. J. W. Edwards, Ann Arbor, Mich., 1946.

47. Heywood, R. B.: Designing by Photoelasticity. Chapman and Hall Ltd., London, 1952.

48. Peterson, R. E.: Notch Sensitivity. McGraw-Hill Book Co. Inc., 1959.

49. Kuguel, R.: The Highly Stressed Volume of Material as a Fundamental Parameter in the Fatigue Strength of Metal Members. Univ. of Ill., T & A.M. Rept. No. 169, June 1960, see also The Relation Between the Theoretical Stress Concentration Factor K_t, and the Fatigue Notch Factor, K_f, According to the Highly Stressed Volume Approach. Univ. of Ill., T & A.M. Rept. No. 184, December 1960.

50. Harris, H. J.: Metallic Fatigue. Pergamon Press, New York, 1961.

51. Raske, D. T.: Section and Notch Size Effects in Fatigue. Univ. of Ill., T & A.M. Rept. No. 360, August 1972.

52. Neuber, H.: Theory of Stress Concentration for Shear Strained Prismatic Bodies with Arbitrary Nonlinear Stress-Strain Law. J. App. Mech., vol. 28, no. 4, December 1961, pp. 544-560.

53. Hardrath, H. F.; and Ohman, L.: A Study of Elastic and Plastic Stress Concentration Due to Notches and Fillets in Flat Plates. NACA TN 1117, 1953.

54. Leis, B. N.: Nonlinear Aspects of Structural Fatigue Damage Assessment and Accumulation. Proc. 4th Int. Conf. Structural Mech. in Reactor Tech., vol. L, August 1977, pp. L3.3/1-13.

55. Landers, C. B.; and Hardrath, H. F.: Results of Axial-Load Fatigue Tests on Electropolished 2024-T3 and 7075-T6 Aluminum Alloy Sheet Specimens with Central Holes. NACA TN 3631, 1956.

56. Roark, R. J.: Formulas for Stress and Strain. McGraw Hill, 1965.

NASA Contractor Report 145312

DISTRIBUTION LIST
NAS1-14171

	No. of Copies
NASA Langley Research Center Hampton, VA 23665 Attn: Report & Manuscript Control Office, Mail Stop 180A Edward P. Phillips, Mail Stop 188E	1 25
NASA Ames Research Center Moffett Field, CA 94035 Attn: Library, Mail Stop 202-3	1
NASA Dryden Flight Research Center P. O. Box 273 Edwards, CA 93523 Attn: Library	1
NASA Goddard Space Flight Center Greenbelt, MD 20771 Attn: Library	1
NASA Lyndon B. Johnson Space Center 2101 Webster Seabrook Road Houston, TX 77058 Attn: JM6/Library	1
NASA Marshall Space Flight Center Marshall Space Flight Center, AL 35812 Attn: Library, AS61L	1
Jet Propulsion Laboratory 4800 Oak Grove Drive Pasadena, CA 91103 Attn: Library, Mail 111-113	1
NASA Lewis Research Center 21000 Brookpark Road Cleveland, OH 44135 Attn: Library, Mail Stop 60-3 Thomas W. Orange, Mail Stop 49-3	1 1
NASA John F. Kennedy Space Center Kennedy Space Center, FL 32899 Attn: Library, NWSI-D	1
National Aeronautics & Space Administration Washington, DC 20546 Attn: RW-3	1
Battelle's Columbus Laboratories 505 King Avenue Columbus, OH 43201 Attn: B. N. Leis S. G. Sampath	1 1

DISTRIBUTION LIST
NAS1-14171

	No. of Copies
Rockwell International Corporation Aircraft Division International Airport Los Angeles, CA 90009 Attn: N. Klimmek	1
Sikorsky Aircraft Stratford, CT 06602 Attn: G. E. Lattin	1
Beckman Instruments, Inc. 1117 California Avenue Palo Alto, CA 94304 Attn: R. S. Carey	1
Aluminum Company of America 1501 Alcoa Building Pittsburgh, PA 15219 Attn: G. E. Nordmark	1
Martin Marietta Aluminum 19200 South Western Avenue Torrance, CA 90509 Attn: W. M. VanDatta	1
Grumman Aerospace Corporation South Oyster Bay Road Bethpage, NY 11714 Attn: A. Gomza R. J. Heitzmann	1 1
Kaiser Aluminum Center for Technology P. O. Box 748 Fort Worth, TX 76101 Attn: R. L. Jones	1
Boeing Commercial Airplane Company P. O. Box 3707 Seattle, WA 98124 Attn: R. J. Doty	1
Rockwell International Corporation Space Division 12214 Lakewood Boulevard Downey, CA 90241 Attn: J. E. Collipriest	1

DISTRIBUTION LIST
NAS1-14171

	No. of Copies
TIMET 1140 Bloomfield Avenue West Caldwell, NJ 07006 Attn: W. H. Heil	1
Lockheed Aircraft Corporation Lockheed-California Company P. O. Box 551 Burbank, CA 91503	1
Lockheed Aircraft Corporation Lockheed-Georgia Company 86 South Cobb Drive Marietta, GA 30063 Attn: E. J. Bateh	1
The Bendix Corporation Energy Controls Division 717 North Bendix Drive South Bend, IN 46620 Attn: R. V. Cervelli	1
University of Florida College of Engineering Department of Materials Science Gainesville, FL 32611 Attn: C. S. Hartley	1
Technische Hogeschool - Delft Vliegtuigbouwkunde Kleiyerweg 1 - Delft, Amsterdam Attn: J. Schijive	1
General Dynamics Corporation Convair Aerospace Division P. O. Box 80847 San Diego, CA 92138 Attn: J. L. Christian	1
Air Force Materials Laboratory Wright-Patterson Air Force Base, OH 45433 Attn: C. L. Harmsworth	1
University of Illinois Department of Theoretical & Applied Mechanics 321 Talbot Laboratory Urbanna, IL 61801 Attn: JoDean Morrow	1

DISTRIBUTION LIST
NAS1-14171

	No. of Copies
McDonnell Douglas Corporation 5301 Bolsa Avenue Huntington Beach, CA 92647 Attn: T. R. Murray	1
University of Akron Engineering Department Akron, OH 44304 Attn: Technical Librarian	1
Northrop Corporation Noair Division 3901 West Broadway Hawthorne, CA 90250 Attn: V. E. Frost	1
Auburn University Auburn, AL 36830 Attn: H. W. Maynor	1
TRW Systems, Inc. 23555 Euclid Avenue Cleveland, OH 44117 Attn: P. N. Randall	1
National Research Council of Canada National Aeronautical Establishment Ottawa, Ontario, CANADA Attn: J. A. Dunsby	1
LTV Aerospace Corporation P. O. Box 5907 Dallas, TX 75222 Attn: S. W. McClaren	1
University of Minnesota Mechanical Engineering Department Minneapolis, MN 55455 Attn: B. J. Lazan	1
National Bureau of Standards U. S. Department of Commerce Washington, DC 20234 Attn: E. M. Marlow/EM 219	1
General Electric Company Aircraft Engine Group Lynn, MA 01905 Attn: J. Miller	1

NASA Contractor Report 145312

DISTRIBUTION LIST
NAS1-14171

	No. of Copies
United Technologies Corporation Pratt & Whitney Aircraft Advanced Materials Research & Development Lab East Hartford, CT 06108 Attn: E. F. Bradley	1
Defense Research Information Centre St. Mary Cray Orpington, Kent UNITED KINGDOM Attn: M. E. Murray	1
NASA Scientific & Technical Information Facility 6571 Elkridge Landing Road Linthicum Heights, MD 21090	31 plus original